by the PAF method remains to be clarified for its implication for Aβ pathology of AD and its mouse models. Notably, the molecular layer of the hippocampal dentate gyrus is the brain region that produces larger amounts of the minute plaques in the APP-SL mice than in the aged humans. This observation might explain partly, albeit not totally, why the retrieving effects differ between the human and mouse brains.

This powerful PAF method could reveal numerous SPs and various Aβ deposits that have not been detected so far. Therefore, the PAF method could serve as a sensitive IHC tool to give new insights into Aβ pathology of AD and its mouse models. We speculate that the PAF method may be the Aβ AR method with the highest efficiency so far and could be used in place of the conventional FA method.

Acknowledgments

We thank H. Kudo and H. Murayama for technical assistance and Daniel Berrar (Tokyo Institute of Technology) for the proofreading of this article and helpful comments.

Declaration of Conflicting Interests

The authors declared no potential conflicts of interest with respect to the research, authorship, and/or publication of this article.

Funding

The authors received the following financial support for the research, authorship, and/or publication of this article: This work was partially supported by the Starter Research Subvention of Tohoku University Graduate School of Medicine and Grant-in-Aid for Scientific Research on Innovative Areas (Comprehensive Brain Science Network) from the Ministry of Education, Science, Sports and Culture of Japan.

References

Ballatore C, Lee VM, Trojanowski JQ. 2007. Tau-mediated neurodegeneration in Alzheimer's disease and related disorders. Nat Rev Neurosci. 8:663–672.

Bataille F, Troppmann S, Klebl F, Rögler G, Stoelcker B, Hofstadter F, Bosserhoff AK, Rummele P. 2006. Multiparameter immunofluorescence on paraffin-embedded tissue sections. Appl Immunohistochem Mol Morphol. 14:225–228.

Battifora H, Kopinski M. 1986. The influence of protease digestion and duration of fixation on the immunostaining of keratins: a comparison of formalin and ethanol fixation. J Histochem Cytochem. 34:1095–1100.

Behrouz N, Defossez A, Delacourte A, Mazzuca M. 1991. The immunohistochemical evidence of amyloid diffuse deposits as a pathological hallmark in Alzheimer's disease. J Gerontol. 46:B209–B212.

Hardy J, Selkoe DJ. 2002. The amyloid hypothesis of Alzheimer's disease: progress and problems on the road to therapeutics. Science. 297:353–356.

Hardy JA, Higgins GA. 1992. Alzheimer's disease: the amyloid cascade hypothesis. Science. 256:184–185.

Huang SN, Minassian H, More JD. 1976. Application of immunofluorescent staining on paraffin sections improved by trypsin digestion. Lab Invest. 35:383–390.

Iwatsubo T, Odaka A, Suzuki N, Mizusawa H, Nukina N, Ihara Y. 1994. Visualization of A beta 42(43) and A beta 40 in senile plaques with end-specific A beta monoclonals: evidence that an initially deposited species is A beta 42(43). Neuron. 13:45–53.

Kang J, Lemaire HG, Unterbeck A, Salbaum JM, Masters CL, Grzeschik KH, Multhaup G, Beyreuther K, Muller-Hill B. 1987. The precursor of Alzheimer's disease amyloid A4 protein resembles a cell-surface receptor. Nature. 325:733–736.

Kitamoto T, Ogomori K, Tateishi J, Prusiner SB. 1987. Formic acid pretreatment enhances immunostaining of cerebral and systemic amyloids. Lab Invest. 57:230–236.

Klunk WE, Xu CJ, Pettegrew JW. 1994. NMR identification of the formic acid-modified residue in Alzheimer's amyloid protein. J Neurochem. 62:349–354.

Lee VM, Balin BJ, Otvos L Jr., Trojanowski JQ. 1991. A68: a major subunit of paired helical filaments and derivatized forms of normal Tau. Science. 251:675–678.

Masters CL, Simms G, Weinman NA, Multhaup G, McDonald BL, Beyreuther K. 1985. Amyloid plaque core protein in Alzheimer disease and Down syndrome. Proc Natl Acad Sci U S A. 82:4245–4249.

Mepham BL, Frater W, Mitchell BS. 1979. The use of proteolytic enzymes to improve immunoglobulin staining by the PAP technique. Histochem J. 11:345–357.

Murayama H, Shin RW, Higuchi J, Shibuya S, Muramoto T, Kitamoto T. 1999. Interaction of aluminum with PHFtau in Alzheimer's disease neurofibrillary degeneration evidenced by desferrioxamine-assisted chelating autoclave method. Am J Pathol. 155:877–885.

Namimatsu S, Ghazizadeh M, Sugisaki Y. 2005. Reversing the effects of formalin fixation with citraconic anhydride and heat: a universal antigen retrieval method. J Histochem Cytochem. 53:3–11.

O'Leary TJ. 2001. Standardization in immunohistochemistry. Appl Immunohistochem Mol Morphol. 9:3–8.

Rocken C, Roessner A. 1999. An evaluation of antigen retrieval procedures for immunoelectron microscopic classification of amyloid deposits. J Histochem Cytochem. 47:1385–1394.

Selkoe DJ. 1991. The molecular pathology of Alzheimer's disease. Neuron. 6:487–498.

Shi SR, Cote RJ, Yang C, Chen C, Xu HJ, Benedict WF, Taylor CR. 1996. Development of an optimal protocol for antigen retrieval: a 'test battery' approach exemplified with reference to the staining of retinoblastoma protein (pRB) in formalin-fixed paraffin sections. J Pathol. 179:347–352.

Shi SR, Key ME, Kalra KL. 1991. Antigen retrieval in formalin-fixed, paraffin-embedded tissues: an enhancement method for immunohistochemical staining based on microwave oven heating of tissue sections. J Histochem Cytochem. 39:741–748.

Downloaded from jhc.sagepub.com at TOHOKU UNIV on January 22, 2013

Shin RW, Iwaki T, Kitamoto T, Tateishi J. 1991. Hydrated autoclave pretreatment enhances tau immunoreactivity in formalin-fixed normal and Alzheimer's disease brain tissues. Lab Invest. 64:693–702.

Shin RW, Kruck TP, Murayama H, Kitamoto T. 2003. A novel trivalent cation chelator Feralex dissociates binding of aluminum and iron associated with hyperphosphorylated tau of Alzheimer's disease. Brain Res. 961:139–146.

Shin RW, Ogino K, Shimabuku A, Taki T, Nakashima H, Ishihara T, Kitamoto T. 2007. Amyloid precursor protein cytoplasmic domain with phospho-Thr668 accumulates in Alzheimer's disease and its transgenic models: a role to mediate interaction of Abeta and tau. Acta Neuropathol. 113:627–636.

Suurmeijer AJ, Boon ME. 1993. Notes on the application of microwaves for antigen retrieval in paraffin and plastic tissue sections. Eur J Morphol. 31:144–150.

Thal DR, Sassin I, Schultz C, Haass C, Braak E, Braak H. 1999. Fleecy amyloid deposits in the internal layers of the human entorhinal cortex are comprised of N-terminal truncated fragments of Abeta. J Neuropathol Exp Neurol. 58:210–216.

Uchihara T, Kondo H, Akiyama H, Ikeda K. 1995. White matter amyloid in Alzheimer's disease brain. Acta Neuropathol. 90:51–56.

Wisniewski HM, Bancher C, Barcikowska M, Wen GY, Currie J. 1989. Spectrum of morphological appearance of amyloid deposits in Alzheimer's disease. Acta Neuropathol. 78:337–347.

Yamamoto A, Shin RW, Hasegawa K, Naiki H, Sato H, Yoshimasu F, Kitamoto T. 2002. Iron (III) induces aggregation of hyperphosphorylated tau and its reduction to iron (II) reverses the aggregation: implications in the formation of neurofibrillary tangles of Alzheimer's disease. J Neurochem. 82:1137–1147.

Downloaded from jhc.sagepub.com at TOHOKU UNIV on January 22, 2013

Journal of the Neurological Sciences 312 (2012) 108–116

Contents lists available at ScienceDirect

Journal of the Neurological Sciences

journal homepage: www.elsevier.com/locate/jns

Creutzfeldt–Jakob disease with the M232R mutation in the prion protein gene in two cases showing different disease courses: A clinicopathological study

Naoya Takeda [a], Osamu Yokota [a,*], Seishi Terada [a], Takashi Haraguchi [b], Keigo Nobukuni [b], Reiko Mizuki [a], Hajime Honda [a], Hidenori Yoshida [a], Yuki Kishimoto [a], Etsuko Oshima [a], Hideki Ishizu [c], Katsuya Satoh [d], Tetsuyuki Kitamoto [e], Yuetsu Ihara [b], Yosuke Uchitomi [a]

[a] Department of Neuropsychiatry, Okayama University Graduate School of Medicine, Dentistry and Pharmaceutical Sciences, Okayama, Japan
[b] Department of Neurology, National Hospital Organization Minami-Okayama Medical Center, Okayama, Japan
[c] Department of Laboratory Medicine and Pathology, Zikei Hospital, Okayama, Japan
[d] Department of Molecular Microbiology and Immunology, Nagasaki University Graduate School of Biomedical Sciences, Nagasaki, Japan
[e] Division of Neurological Science, Department of Prion Research, Tohoku University Graduate School of Medicine, Sendai, Japan

ARTICLE INFO

Article history:
Received 25 April 2011
Received in revised form 12 July 2011
Accepted 4 August 2011
Available online 7 October 2011

Keywords:
Creutzfeldt–Jakob disease
Genetic prion disease
Immunohistochemistry
M232R
Prion
Western blotting

ABSTRACT

We report two autopsy cases of Creutzfeldt–Jakob disease (CJD) with the M232R mutation of the prion protein (PrP) gene that exhibited different clinicopathological features (age at death, 64/54 years; disease duration, 13/26 months). Both cases showed myoclonus, hyperintensity on diffusion-weighted MRI, and increased 14-3-3 protein in the cerebrospinal fluid. The initial sign in each case was memory disturbance and abnormal pharyngeal sensation, respectively. In the first case, the disease progressed rapidly with akinetic mutism developing 6 months after onset, while it occurred 23 months after onset in the second case. Pathologically, both cases had severe neuronal loss with gliosis and spongiform change in the cerebral cortex, basal ganglia, and cerebellum. PrP deposition was the diffuse synaptic type in the first case, but the second case had both diffuse synaptic and perivacuolar types. PrP^{sc} immunoblotting revealed a type 1 band pattern in the first case, but both types 1 and 2 in the second case. Based on these findings, together with the results in previous CJD cases with M232R, we noted the possibility that the presence of type 2 PrP^{sc} may be associated with both morphological features of PrP deposition and slow disease progression in this genetic prion disease.
© 2011 Elsevier B.V. All rights reserved.

1. Introduction

Human prion diseases are a group of rare fatal neurodegenerative conditions characterized by accumulation of an abnormal conformation of prion protein (PrP^{sc}) [1–3]. Approximately 80–90% of prion disease cases lack any mutation in the prion protein gene (*PRNP*), i.e., sporadic Creutzfeldt–Jakob disease (sporadic CJD), while about 10–20% of cases are affected by a genetic form. Currently, the latter cases are classified into four major clinicopathological phenotypes: genetic Creutzfeldt–Jakob disease (genetic CJD), Gerstmann–Sträussler–Scheinker disease (GSS), fatal familial insomnia, and PrP cerebral amyloid angiopathy [4–6]. Based on the results of the EUROCJD surveillance, a cross-regional study that was carried out in European countries, Australia, and Canada, the most frequent mutation in genetic prion diseases was E200K (38.5%), followed by V210I (15.2%), D178M (3.5%), E196K (1.1%), V203I (1.1%), and E211Q (0.9%) [5].

On the other hand, it was reported that the frequencies of variable mutations in *PRNP* in Japanese patients with genetic prion diseases may be different from those observed in western countries: the most frequent mutation in Japanese patients was reported to be V180I (41.2%), followed by P102L (18.1%) and E200K (17.1%). The point mutation of ATG (methionine) to AGG (arginine) at codon 232 in *PRNP*, M232R, is the most fourth frequent mutation in Japanese patients with genetic prion disease (approximately 15%) [7]. In sporadic CJD, it is considered that the combination of the polymorphism at codon 129 (methionine/methionine [MM], valine/valine [VV] homozygosity, or methionine/valine [MV] heterozygosity) and two different-sized non-glycosylated protease-resistant PrP core fragments (i.e., type 1 and type 2) may affect the clinical and pathological characteristics presented in each case (i.e., the MM1, MM2, MV1, MV2, VV1, and VV2 molecular types, according to Parchi's classification) [8–12]. Shiga et al. [13] recently examined the clinical pictures of 20 patients with CJD associated with M232R (CJD M232R), including 8 autopsied cases, and noted the possibility that cases having this mutation exhibit two different clinical subtypes with respect to the rate of disease progression: cases showing rapidly or slowly progressive disease courses. No previous CJD case with M232R had a family history. In their study, the clinical features of rapidly progressive cases with M232R

* Corresponding author at: Department of Neuropsychiatry, Okayama University Graduate School of Medicine, Dentistry and Pharmaceutical Sciences, 2-5-1 Shikata-cho, Okayama 700-8558, Japan.
E-mail address: oyokota1@yahoo.co.jp (O. Yokota).

0022-510X/$ – see front matter © 2011 Elsevier B.V. All rights reserved.
doi:10.1016/j.jns.2011.08.008

were reminiscent of those in cases with the MM1 subtype sporadic CJD (i.e., frequently the initial sign is dementia, with rapidly progressive neurological abnormalities, including myoclonus, ataxia, and visual abnormalities developing subsequently, and the total disease duration is about 4 months) [7,12–23]. In contrast, the slow-type cases were considered clinically similar to the MM2 cortical subtype of sporadic CJD (i.e., cognitive impairment is frequently the initial symptom, myoclonus and pyramidal signs often develop later, ataxia is less common, and the total disease course is significantly longer, about 20 months) [7,12,13,23–29]. However, because only a small number of autopsy cases have been reported, what genetic, molecular, or immunohistochemical factors modify or predict the clinical presentation in CJD patients with M232R remains unclear.

We here report two autopsied CJD cases bearing M232R that showed different clinical, biochemical, and histopathological characteristics. Then we review previously reported CJD cases having the same mutation, and discuss the potential relationship between clinical, biochemical, and histopathological features in CJD with M232R.

2. Case reports

2.1. Case 1

A 63-year-old Japanese man first developed memory disturbance, and 2 months after onset, difficulty in understanding conversations and recognizing acquaintances' faces also occurred. Subsequently, his intelligence rapidly deteriorated. Four months after onset, disorientation, gait disturbance, and difficulty in speaking occurred. The first neurological examination 5 months after onset revealed myoclonus, ataxic gait, dysarthria, and dysgraphia. Hyperreflexes, Babinski sign, tremor, or rigidity was not noted. He had no family history or no relevant past medical history, including a dura mater graft or corneal transplant. He scored 3/30 on the Mini Mental State Examination. Routine examinations of blood and urine were unremarkable. An electroencephalogram (EEG) showed typical periodic sharp-wave complexes (PSWCs). Brain MRI revealed high signal intensity in the bilateral temporal and parietal, and to a lesser degree, in the frontal and occipital cortices on fluid-attenuated inversion recovery (FLAIR) images and diffusion-weighted images (DWI), but without evident cerebral atrophy (Fig. 1a and b). In a cerebrospinal fluid (CSF) examination, a cell count was normal, the total tau protein was elevated, and 14-3-3 protein assay was positive. A PrP^{sc} amplication assay using the real-time quaking-induced conversion method [30] demonstrated PrP^{sc} in the CSF. Genetic analysis of *PRNP* revealed an ATG (methionine) to AGG (arginine) point mutation at codon 232 (M232R), homozygous methionine (Met/Met) at codon 129, and homozygous glutamate (Glu/Glu) at codon 219. Within 1 week after admission, he could not stand without support and became bedridden. Thereafter, he needed tube feeding, and developed akinetic mutism 6 months after onset. Brain MRI at 9 months after onset showed diffuse cortical atrophy, dilation of both lateral ventricles, and moderate atrophy in the caudate nucleus. In addition, periventricular hyperintensity on FLAIR images and bilateral insular cortices hyperintensity on DWI were observed (Fig. 1c and d). He died of pneumonia and sepsis at the age of 64 with a clinical course of 13 months.

2.2. Case 2

A 51-year-old Japanese man initially complained of an abnormal pharyngeal sensation. Three months later lightheadedness and 6 months later double vision occurred, and his intelligence gradually declined. His first neurological examination revealed mild gait disturbance and ataxia. His spontaneous speech output was apparently reduced 10 months after onset. He was admitted to the hospital

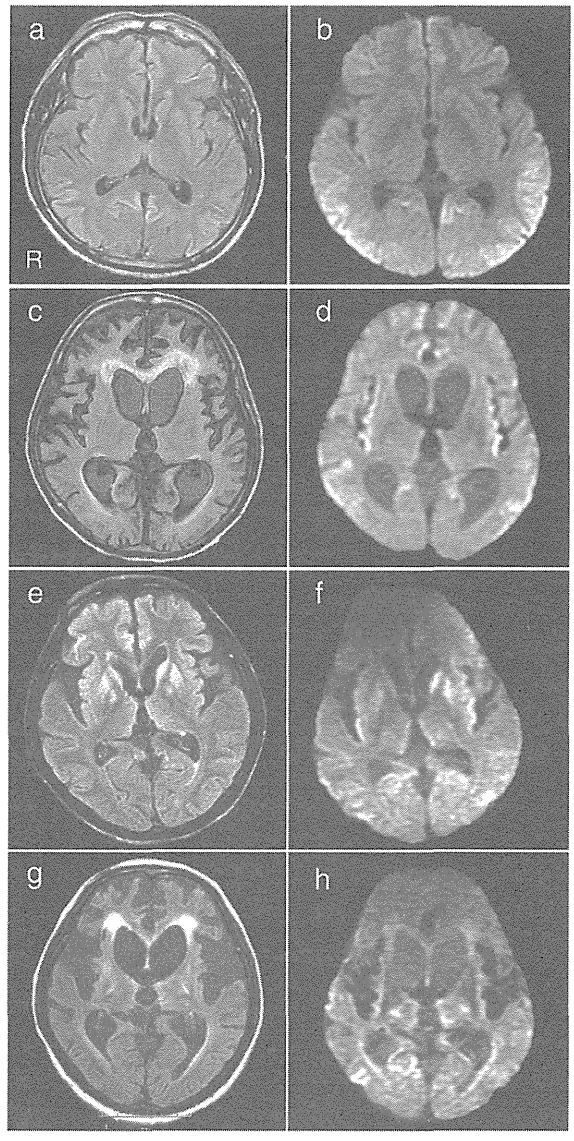

Fig. 1. Brain MR imaging (MRI); fluid-attenuated inversion recovery (FLAIR) and diffusion weighted images (DWI). (a,c,e,g) FLAIR images, (b,d,f,h) DWI. (a–d) Case 1. (a, b) Brain MRI at 6 months after onset shows no obvious brain atrophy, but revealed increased signal intensity in the bilateral temporal and parietal cortices, and to a lesser degree, in the frontal and occipital cortices. (c,d) Brain MRI at 9 months after onset shows marked cortical atrophy and dilation of both lateral ventricles. Additionally, periventricular hyperintensity on FLAIR images and increased signal in bilateral insular cortices on DWI are also noted. (e–h) Case 2 (e,f) A FLAIR image at 13 months after onset shows increased signal intensity in the bilateral frontal and insular cortices, striatum, pallidum, and thalamus on FLAIR. In addition, in DWI, increased signal in bilateral temporal, parietal, and occipital cortices is noted. (g,h) Brain MRI at 23 months after onset shows marked atrophy in the neocortices and basal ganglia. Marked dilation of the both lateral ventricles and periventricular hyperintensity are also noted.

13 months after onset. At the time, he could not sit without support. He showed moderate difficulty in swallowing, mutism, ataxic movement, and increased deep tendon reflexes. He had no family history or no relevant past medical history, including a dura mater graft or corneal transplant. No pathological reflex, including Babinski sign or muscle weakness, was found. Routine blood examination was unremarkable. Brain MRI showed frontal-predominant cerebral atrophy with high signal intensity lesions in the cerebral cortex and basal ganglia on FLAIR images and DWI (Fig. 1e and f). The CSF was

positive for 14-3-3 protein. Analysis of *PRPN* revealed an M232R substitution, Met/Met at codon 129, and Glu/Glu at codon 219. Fourteen months after onset, bilateral upper-limb myoclonus occurred. He developed akinetic mutism 23 months after onset. Brain MRI showed severe atrophy in the cerebral cortices, basal ganglia with marked dilation of both lateral ventricles (Fig. 1g and h). He died of sepsis at the age of 54 after a clinical course of 26 months. An EEG showed no PSWCs throughout the course.

3. Materials and methods

3.1. Neuropathological examination

The brain was fixed in 10% buffered formalin, and tissue blocks were immersed in 95% formic acid to inactivate the PrP. Ten-μm-thick sections were prepared from representative anatomical regions and stained by the hematoxylin-eosin (H&E), Klüver–Barrera, modified Bielschowsky silver, and Gallyas–Braak silver methods. The severity of spongiform change and the presence or absence of confluent vacuoles were assessed.

Then sections were immunostained by the immunoperoxidase method using 3′3-diaminobenzidine tetrahydrochloride. Antibodies used were against PrP (3F4, mouse, monoclonal, 1:1000, Covance Research Products Inc. (formerly Signet Laboratories), Princeton, NJ, USA), phosphorylated tau (AT8, mouse, monoclonal, 1:1000, Innogenetics, Ghent, Belgium), amyloid β42 (Aβ42, rabbit, polyclonal, 1:100, Immuno-Biological Laboratories, Takasaki, Japan), phosphorylated α-synuclein (psyn#64, mouse, monoclonal, 1:5000, Wako, Osaka, Japan), and phosphorylated TDP-43 (pS409/410–2, rabbit polyclonal, 1:5000, Cosmo Bio, Tokyo, Japan). For the PrP immunohistochemistry, deparaffinized sections were pretreated by hydrolytic autoclaving in 1.5 mM HCl at 121 °C for 10 min as described previously [31]. When using anti-Aβ42 and -psyn#64, sections were pretreated with 70% formic acid for 10 min for antigen retrieval. The morphological features of PrP deposition were assessed in eight recommended regions, comprising the frontal, temporal, parietal, and occipital cortices, hippocampus, striatum, thalamus, and cerebellar cortex [11].

3.2. PrP gene analysis

Genomic DNA was extracted from lymphocytes in the peripheral blood and used to amplify the open reading frame of the PrP gene by PCR, as described previously [32,33].

3.3. Western blot analyses

Frozen tissues obtained from the right frontal cortex were homogenized. Western blot analysis of protease-resistant PrP^{sc} was performed using 3F4 (mouse, monoclonal, 1:10,000), Tohoku 1 (T1, rabbit, polyclonal, 1:5000), and Tohoku 2 (T2, rabbit, polyclonal, 1:3000), antibodies as described previously [34,35]. Typing of PrP^{sc} was performed on the basis of the classification system proposed by Parchi et al. [8–12].

4. Results

4.1. Case 1

The brain weighed 1336 g before fixation. Macroscopically, the cerebrum was mildly swollen due to cerebral edema resulting from

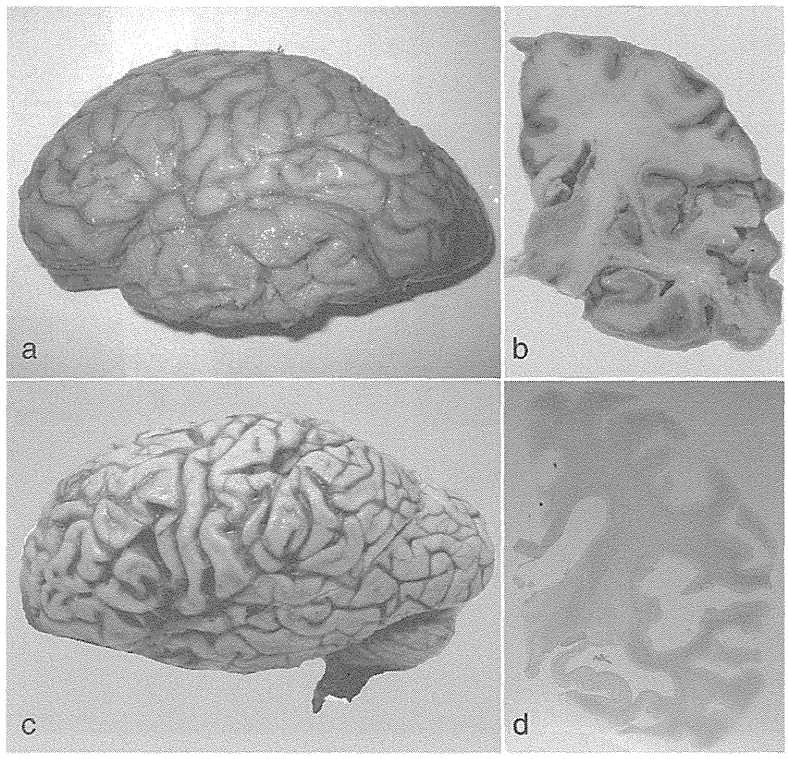

Fig. 2. Macroscopic findings. (a) The cerebrum is mildly swollen because cerebral edema developed in the terminal stage. (b) Severe atrophy in the cortical ribbon and severe tissue rarefaction in the striatum. The volume of the hippocampus is relatively well spared. (c) Diffuse atrophy accentuated in the frontal, temporal, and parietal lobes. The cerebellum is also atrophic. (d) A coronal section at the level of the mammillary body. Severe atrophy is seen in the frontal and temporal cortices and basal ganglia. Myelin pallor in the cerebral white matter is also evident. (a,b) case 1, (c,d) case 2.

acute bacterial leptomeningitis associated with the sepsis that developed in the terminal stage, being inconsistent with MRI findings in life (Fig. 2a). However, a coronal section showed severe atrophy in the cortical ribbon. The striatum showed severe tissue rarefaction. The volume of the hippocampus was relatively well spared (Fig. 2b). The substantia nigra was well pigmented. The pons, medulla oblongata, and cerebellum were unremarkable.

Microscopically, moderate to neuronal loss associated with remarkable proliferation of hypertrophic astrocytes was noted in extensive regions in the cerebral cortex (Fig. 3a). Spongiform changes such as microvacuolar changes, were observed in the cerebral and cerebellar cortices (Table 1). The cerebral white matter was also severely involved with proliferation of hypertrophic astrocytes. The amygdala showed moderate neuronal loss and tissue rarefaction. In the putamen, severe neuronal loss with marked tissue rarefaction, glial proliferation, and status spongiosus were noted. The globus pallidus and the thalamus showed moderate neuronal loss associated with astrocyte proliferation and status spongiosus. In the tegmentum of the brain stem, tissue rarefaction with glial proliferation was evident. The brain stem nuclei were relatively well preserved except for the pontine nucleus, in which astrocytes and microglia were proliferated. The pyramidal tract in the medulla was spared. In the cerebellum, the molecular layer showed tissue rarefaction with mild spongiform change, and the granular cell layer showed severe

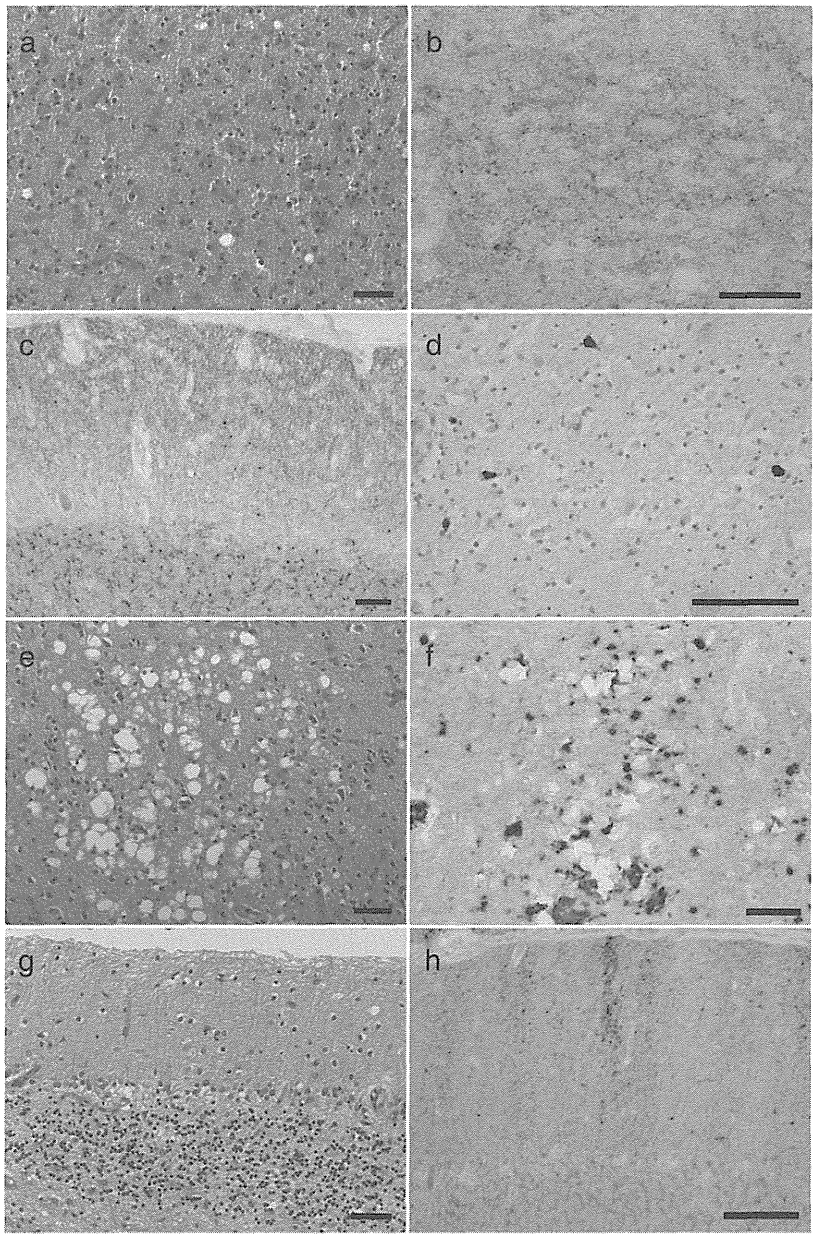

Fig. 3. Microscopic findings of representative lesions. (a) Severe neuronal loss and hypertrophic astrocytes are evident in the frontal cortex. (b) Synaptic PrP deposition in the frontal cortex. (c) Synaptic PrP deposition in the cerebellar cortex, involving both molecular and granular cell layers. No plaque-type PrP deposition was observed. (d) Neurofibrillary tangles in the amygdala. (e) Confluent vacuolar spongiform change in the occipital cortex. (f) A serial section of (e). Perivacuolar PrP deposition in the occipital cortex. (g) Loss of Purkinje cells and proliferation of Bergmann glia with a moderate loss of granular cells in the cerebellar cortex. (g) Synaptic PrP deposition with irregular linear deposition in the molecular cell layer in the cerebellar cortex. (a–d) Case 1, (e–h) case 2. (a,e,g) Hematoxylin and eosin stain, (b,c,f,h) 3F4 immunohistochemistry, (d) AT-8 immunohistochemistry. All scale bars = 50 μm.

Table 1
Summary of clinical and pathological characteristics of present cases.

	Case 1	Case 2
Sex	M	M
Age at onset (y)	63	51
Age at death (y)	64	54
Total disease duration (m)	13	26
Duration from disease onset to akinetic mutism (m)	6	23
Initial symptom	Memory disturbance	Abnormal pharyngeal sensation
Periodic sharp-wave complex	Present	None
High signal on diffusion weighted images	Present	Present
14-3-3 protein in cerebrospinal fluid	Positive	Positive
PrP^{sc} in cerebrospinal fluid	Positive	N.E.
PRNP mutation	M232R	M232R
Codon 129	Met/Met	Met/Met
Codon 219	Glu/Glu	Glu/Glu
Pathological findings (microvacuolar spongiform change/confluent vacuoles/PrP immunostaining)		
Frontal cortex	+/−/synaptic	+/−/synaptic
Temporal cortex	+/−/synaptic	+/+/synaptic, perivacuolar
Parietal cortex	+/−/synaptic	+/+/synaptic, perivacuolar
Occipital cortex	+/−/synaptic	+/+/synaptic, perivacuolar
Striatum	+/−/synaptic	+/−/synaptic
Hippocampus	−/−/synaptic	−/−/−
Thalamus	+/−/synaptic	+/−/synaptic
Cerebellar cortex	+/−/synaptic	+/−/synaptic
PrP^{sc} immunoblotting	Type 1	Type 1 + type 2

M, male; N.E., not examined; synaptic, diffuse synaptic PrP deposition; perivacuolar, perivacuolar PrP deposition.

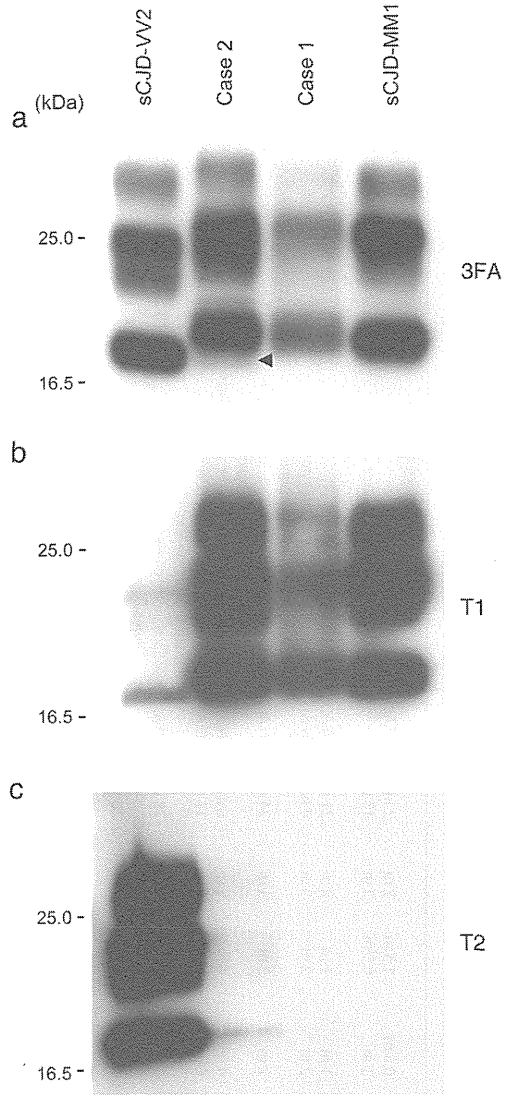

Fig. 4. Western blot analysis of PrP^{sc} using PrP^{sc} type-specific antibodies: type 1 PrP^{sc}-specific polyclonal antibody Tohoku 1 (T1), type 2 PrP^{sc}-specific polyclonal antibody Tohoku 2 (T2). 3F4 antibody detects both PrP^{sc} types. The present cases are shown flanked by standard samples of sporadic CJD MM1 (sCJD MM1) and sporadic CJD VV2 (sCJD VV2). (a) Western blot analysis using 3F4 in the right frontal cortex from case 1 shows the type 1 PrP^{sc} band pattern similar to that observed in sCJD MM1. In addition to the type 1 PrP^{sc} band pattern, a faint type 2 PrP^{sc} band (arrowhead) is detected in the right frontal cortex from case 2. (b) Western blot analysis using T1 of the right frontal cortex from cases 1 and 2 shows the same band pattern as sCJD MM1. T1 also reveals the minority subpopulations in the sCJD VV 2 brain that can be detected by type 1 PrP^{sc}-specific antibodies, as reported previously [35]. (c) Western blot analysis using T2 of the right frontal cortex from case 2 shows a T2-reactive PrP^{sc} band pattern as well as sCJD VV2. No band is seen in case 1 and sCJD MM1.

neuronal loss, while the Purkinje cells were relatively preserved. The neurons in the dentate nucleus were not reduced in number, although astrocyte proliferation was noted.

In addition to these features of CJD, this case also had histopathological alterations that were probably due to the acute bacterial meningitis and hypoxia that developed in the terminal stage. That is, in the hippocampus, the pyramidal neurons in the CA1 were severely reduced in number with tissue rarefaction. Neuronal loss with glial proliferation in the hippocampal dentate gyrus was also found. Microbleeding with and without necrosis was often noted in the amygdala, temporal pole, and pons.

Immunohistochemical analysis with 3F4 revealed diffuse synaptic-type deposition in the cerebral cortices, hippocampus, amygdala, basal ganglia, thalamus, inferior olivary nucleus, and cerebellum (Fig. 3b and c). Neither plaque- nor perivacuolar-type deposition was observed in any region. AT-8 immunohistochemistry demonstrated a small number of neurofibrillary tangles in the amygdala, hippocampus, and tegmentum of the pons and midbrain (Fig. 3d). No Aβ deposition, α-synuclein pathology, argyrophilic grains, or TDP-43-positive lesions were found in any region.

Western blot analysis of the PrP^{sc} in the right frontal cortex showed a type 1 band pattern (Fig. 4).

4.2. Case 2

The brain weighed 890 g after fixation. Macroscopically, diffuse atrophy was evident in the frontal, temporal, and parietal lobes. The cerebellum was also atrophic (Fig. 2c). The brain stem showed marked atrophy; however, the substantia nigra was well pigmented. Microscopic examination demonstrated severe neuronal loss associated with astrocyte proliferation and status spongiosus in the extensive regions in the cerebral cortex. In addition to microvacuolar spongiform changes, confluent spongiform changes were also observed in the temporal, parietal, and occipital cortices (Fig. 3e). The hippocampal pyramidal neurons were relatively well spared in number. The thalamus was macroscopically severely atrophic, and microscopically, neuronal loss associated with astrocyte proliferation and status spongiosus were evident. Neuronal loss with astrocyte proliferation and status spongiosus were also found in the putamen and globus pallidus. In the substantia nigra, although tissue rarefaction was evident, pigmented neurons were relatively preserved in number. The pyramidal tract at the level of the midbrain was degenerated. Neuronal

Table 2
Previous CJD232 cases with mutation in PrP gene.

No. [Ref.]	Age at onset (y)	Sex	Brain weight (g)	Initial symptoms	Myoclonus[a]	PSWCs[a]	Akinetic mutism[a]	Disease duration	CSF findings (14-3-3)	Neuropathological findings	Tau pathology	PrP-ir[b]	PrP^{SC} type	Codon 129
Rapid-type cases														
1 [22]	70	M	N.A.	Cerebellar ataxia, hand tremor	0.5 m	1.5 m	2 m	2 m	N.A.	N.A.	N.A.	N.A.	N.A.	M/M
2 [17]	68	M	1100	Dementia	1 m	0.5 m	2 m	13 m	+	Typical spongiform change and status spongiosus, no kuru plaque	N.A.	Synaptic	Type 1	M/M
3 [14]	67	F	870	Weakness of hand	1 m	1 m	2 m	21 m	N.A.	MM1-type sCJD-like	N.A.	N.A.	N.A.	N.A.
4 [16]	55	M	1005	Gait disturbance, disorientation	2 m	2 m	3 m	4 m	N.A.	Spongiform change, astrocytosis, neuronal loss, no kuru plaque	No NFT	Synaptic	N.A.	M/M
5 [16]	64	M	710	Writer's cramp, gait disturbance	2 m	3 m	3 m	24 m	N.A.	Spongiform change, astrocytosis, neuronal ross, no kuru plaque	No NFT	Synaptic	N.A.	M/M
6 [18]	68	M	1210	Difficulty in writing and dressing	4 m	4 m	5 m	6 m	N.A.	Diffuse spongiform change, astrocytosis	N.A	+[c]	N.A.	N.A.
7 [15]	84	M	N.A.	Disorientation	6 m	N.A.	6 m	12 m	N.A.	Spongiform change, astrocytosis, neuronal loss, no kuru plaque	N.A.	Synaptic	N.A.	N.A.
8 [16]	70	F	700	Disorientation	7 m	7 m	7 m	20 m	N.A.	Spongiform change, astrocytosis, neuronal loss, no kuru plaque	No NFT	Synaptic	N.A.	M/M
9 [19]	71	F	700	Memory disturbance	6 m	7 m	7 m	20 m	N.A.	Severe neuronal loss and gliosis, severe spongiform change	N.A.	Synaptic	N.A.	N.A.
10 [20]	50	F	N.A.	Visual symptoms	7 m	7 m	8 m	N.A[d]	N.A.	N.A.	N.A.	N.A.	N.A.	N.A.
11 [21]	N.A.	N.A.	N.A.	N.A.	N.A.	N.A.	N.A.	N.A.	N.A.	N.A.	N.A.	Synaptic	Type 1	N.A.
12[e]	63	M	1336	Memory disturbance	5 m	5 m	6 m	13 m	+	Micro-vacuolar spongiform change, astrocytosis, neuronalloss, no kuru plaque	+[f]	Synaptic	Type 1	M/M
Slow-type case														
1 [27]	63	F	N.A.	Difficulty in dressing	–	13 m	18 m>	18 m[d]	N.A.	N.A.	N.A.	Perivacuolar, synaptic	Type 1 + 2	N.A.
2 [29]	69	M	900	Agraphia, memory disturbance	5 m	30 m	23 m	37 m	+	spongiform change with large confluent vacuolar, no kuru plaque	+[g]	Perivacuolar, plaque	Type 2	M/M
3 [25]	53	F	N.A.	Memory disturbance	11 m	29 m	36 m	N.A[d]	N.A.	N.A.	N.A.	N.A.	N.A.	N.A.
4 [28]	50	M	1270	Memory disturbance	–	–	–	7 m	N.A.	spongiform change with large confluent vacuolar, no kuru plaque	N.A.	Perivacuolar	N.A.	M/M
5 [26]	70	M	N.A.	Memory disturbance	–	–	–	N.A[d]	N.A.	N.A.	N.A.	N.A.	N.A.	N.A.
6 [24]	65	M	N.A.	Memory decline, gait disturbance	N.A.	–	–	16 m	+	N.A.	N.A.	N.A.	N.A.	M/M
7[h]	54	M	890	Abnormal pharyngeal sensation	14 m	–	23 m	26 m	+	Microvacuolar and confluent spongiform changes, astrocytosis, neuronal loss, no kuru plaque	+[i]	Perivacuolar, synaptic	Type1 + 2	M/M
Unclassifiable case														
1 [37]	44	M	N.A.	Perseverative speech, behavioral changes	N.A.	N.A.	N.A.	36 m	N.A.	N.A.	N.A.	N.A.	N.A.	N.A.

M, male; F, female; N.A., not available; m, months; M/M, methionine/methionine; NFT, neurofibrillary tangle; PSWCs, periodic sharp wave complexes.
[a] The duration from the onset until the appearance of each symptom.
[b] PrP immunoreactivity.
[c] Briefly described as PrP deposition.
[d] Patients were still alive at the time of reporting.
[e] Present case 1.
[f] A few neurofibrillary tangles in the basolateral amygdala, hippocampus and tegmentum of the pons and midbrain.
[g] Braak AT8 stage II.
[h] Present case 2.
[i] A few neurofibrillary tangles and neuropil threads in the transentorhinal region, CA1, and subiculum.

loss and gliosis were observed in the pontine nucleus and tegmentum of the pons, while neurons in the locus coeruleus were not reduced in number. In the medulla, the pyramidal tract was evidently degenerated, and neurons in the inferior olivary nucleus had almost completely disappeared. In the cerebellum, Purkinje cell loss and proliferation of Bergmann glia were evident and the granular cell layer showed moderate neuronal loss (Fig. 3g).

PrP immunohistochemistry revealed diffuse synaptic-type deposition in extensive regions in the cerebral cortex, thalamus, basal ganglia, hippocampus, and cerebellum. In addition, perivacuolar-type deposition was found in the temporal, parietal, and occipital cortices (Fig. 3f). In the molecular cell layer of the cerebellum, diffuse synaptic-type accumulation and irregular linear deposition of PrP were noted (Fig. 3h). No plaque-type deposition was observed in any region. AT-8 immunohistochemistry demonstrated a few neurofibrillary tangles and neuropil threads in the transentorhinal region, and the CA1 and subiculum in the hippocampus. No Aβ deposition, α-synuclein pathology, argyrophilic grains, or TDP-43-positive lesions were found in any region.

Western blot analysis of the PrP^{sc} in the right frontal cortex showed a type 1 + 2 band pattern (Fig. 4).

The distribution patterns of pathological changes in both cases are summarized in Table 1.

5. Discussion

We report two Japanese cases of CJD M232R with a codon 129 MM. Both cases had an identical mutation in *PRNP*, but showed evidently different clinical and neuropathological features. The most prominent difference in the clinical presentation was the rate of disease progression: case 1 showed a rapidly progressive disease course similar to that in sporadic CJD MM1, while case 2 showed a relatively slow progression. Pathologically, both cases had very similar distributions and severity of the spongiform changes in the cerebrum and cerebellum; however, case 1 had microvacuolar changes and case 2 had confluent vacuoles, respectively. In addition, the two cases had different combinations of PrP immunostaining patterns and PrP^{sc} molecular types: synaptic PrP deposition and PrP^{sc} type 1 in case 1, and both synaptic and perivacuolar PrP deposition as well as PrP^{sc} type 2 in case 2.

Based on a recent report by the Creutzfeldt–Jakob Disease Surveillance Committee in Japan, the M232R mutation is the fourth most frequent disease-specific mutation in the *PRNP* gene in Japanese patients with genetic prion disease (approximately 15.3%) [7]. To our knowledge, only 12 autopsy cases of CJD with the M232R mutation have been reported (Table 2) [13–19,21,27–29]. This mutation has not been reported in any European country, Canada, or Australia [5,6], and almost all of the cases having this mutation were Japanese [7,13–22,24–29,36,37].

In sporadic CJD, there is agreement that the codon 129 genotype, PrP^{sc} molecular types, and the combination of both may be associated with specific clinical, histopathological, and PrP immunohistochemical features [10–12,38]. Although not conclusive, several previous findings in genetic CJD suggest that the codon 129 genotype and PrP^{sc} molecular types may also modify the clinical and histological phenotypes in genetic CJD cases, like sporadic CJD cases [23]. Consistent with this view, the distribution and morphologic features of spongiform changes in case 1 (MM1) were consistent with that in sporadic CJD MM/MV 1 [12]: the neocortex, striatum, thalamus, and cerebellum showed variable severity of microvacuolar spongiform changes, while the hippocampus and brainstem nuclei were relatively spared. The histopathological features of spongiform changes in case 2 (MM1 + 2) were very similar to that in sporadic CJD MM/MV 1 + 2C [12]: micro-vacuolar spongiform changes with or without confluent vacuoles were observed in the neocortex, striatum, thalamus, and cerebellum, but not in the hippocampus and brainstem nuclei.

As shown in Table 2, of the 20 CJD cases with M232R reported previously, including our two cases, 14 were examined pathologically. Immunohistochemical data on PrP accumulation were available in 13 cases, while PrP^{sc} typing was done only in six of 13 cases. Cooccurrence of type 1 and type 2 PrP^{sc} has been reported in about 10–40% of patients with sporadic CJD [10–12,39,40]. In addition, Puoti et al. [39] reported that the presence of PrP^{sc} type 2 may be associated with the development of perivacuolar PrP deposition in sporadic CJD cases. Likewise, in a recent classification of sporadic CJD, the perivacuolar PrP deposition was noted as an immunohistochemical feature in sporadic CJD cases with PrP^{sc} type 2, such as cases of MM/MV 2C, MM/MV 1 + 2C, and MV2K + 2C [11]. As far as we know, there are only four previously reported CJD cases with M232R in which both PrP immunohistochemical features and PrP^{sc} molecular types were examined: two cases with PrP^{sc}type 1 alone had synaptic type PrP deposition, one case with both PrP^{sc} type 1 and type 2 had synaptic plus perivacuolar PrP deposition, and the other one with PrP^{sc} type 2 alone had perivacuolar-type and plaque-type PrP depositions [13,17,29]. Consistent with these previous findings, our case with PrP^{sc} type 1 had synaptic PrP deposition, while our other case bearing both PrP^{sc}type 1 and type 2 had synaptic plus perivacuolar PrP deposition. That is, the molecular–pathological correlation between PrP^{sc} type 2 and perivacuolar PrP deposition that has been reported in sporadic CJD was also found in all of the six autopsied CJD cases with M232R, including our cases. Given these findings, the PrP^{sc} molecular type may be associated with the pathological phenotype including PrP deposition patterns in CJD cases with M232R, as in sporadic CJD cases.

It is known that most of the CJD cases with M232R exhibit rapid progression of the disease course, while some CJD cases with M232R can show relatively slow progression. In a case series reported by Shiga et al. [13], 15 of 20 CJD cases with M232R (75%) showed rapid disease progression (rapid-type; the period from the onset to the development of akinetic mutism was 3.1 ± 1.5 months), while five cases (25%) showed slow disease progression (slow-type; 20.6 ± 4.4 months). In that study, of the four rapid-type cases in which immunohistochemical data were available, all had synaptic PrP deposition. Further, one rapid-type case in which immunoblotting data were available showed type 1 PrP^{sc}. In contrast, two of the three slow-type cases examined immunohistochemically had perivacuolar PrP deposition in addition to the synaptic pattern, and one had synaptic PrP deposition alone. Further, one case bearing synaptic and perivacuolar PrP deposition had both types 1 and 2 PrP^{sc}[13,29]. Consistent with these results, another previously reported slow-type case [29] and our case 2 also had perivacuolar PrP deposition and type 2 PrP^{sc}. Given these findings, it is plausible that the presence of type 2 PrP^{sc} may be associated with the development of the perivacuolar PrP staining pattern and the slow disease progression in CJD with M232R. In sporadic CJD, however, both MM/MV 1 + 2C and MM/MV 1 cases showed a similar short disease duration, being inconsistent with the potential correlation in M232R cases mentioned above [11,12]. Considering that our case 2 showed the slow disease progression despite having a large amount of type 1 PrP^{sc}, the progression rate might not be simply associated with the amount of type 1 PrP^{sc} deposited at the time of death. There may be other unknown factors, such as the time when deposition of type 1 and/or type 2 PrP^{sc} begins during the course, that influence the disease progression rate in M232R cases. It should be also considered that the amounts and ratio of types 1 and 2 PrP^{sc} are not always identical between anatomical regions. In this study, the amount of type 2 PrP^{sc} in case 2 was very low, as demonstrated in Fig. 4. One possible explanation for the scarcity of type 2 PrP^{sc} presented is that the frontal cortex, in which neither confluent vacuoles nor perivacuolar PrP deposits were observed in case 2, was used for Western blotting. Although frozen tissue from only the frontal lobe was available in our cases, PrP^{sc} typing of several regions such as the temporal, parietal, and occipital cortices, and medial thalamus is preferable, as recommended previously. [11,12]. In association with this issue, Kobayashi et al. [41] recently reported

that even the minority type 2 PrP^{sc} could be consistently detected in sporadic CJD MM1 cases when analyzed with an anti-type 2 PrP^{sc}-specific antibody. Whether the amount of type 2 PrP^{sc} or the ratio of type 1 PrP^{sc} affects the clinical presentation in CJD cases with M232R needs to be explored.

The accumulation of tau pathology was previously reported to be found in GSS cases bearing some mutations (e.g., P105L, A117V or F198S) [42,43]. Kovacs et al. [44] reported that tau-positive neurites were found in 92% of CJD with the E200K mutation, and neurofibrillary changes in 38%. Reiniger et al. [45] also noticed that phosphorylated tau accumulation occurs consistently in sporadic CJD cases. Our two cases had tau-positive lesions in the limbic region. Likewise, among four previous CJD cases with M232R in which tau pathology was evaluated, one had mild tau pathology. Although this concurrent tau pathology might be incidental, the frequency of tau pathology in CJD with M232R should be explored in a larger case series to understand its pathophysiological significance.

In conclusion, although available data are limited at present, taking previous findings together with our results, it is plausible that the clinical features of CJD cases with M232R may be associated with several factors, especially PrP immunohistochemical features and PrP^{sc} molecular type. Further accumulation of clinical, neuropathological, and biochemical findings in autopsy cases of CJD with M232R is needed to clarify the pathogenesis of this disease, to confirm the significance of an M232R mutation, and to provide the more precise information regarding the prognosis to clinicians and families.

Conflict of interest

None of the authors have any conflict of interest.

Acknowledgment

We would like to thank Ms. Onbe (Department of Neuropsychiatry, Graduate School of Medicine, Dentistry, and Pharmaceutical Sciences Okayama University) for her excellent and proficient technical assistance. Brain tissues were obtained from the Research Resource Network, which was supported by a Research Grant for Neurological and Mental Disorders from the Ministry of Health, Labour and Welfare, Japan. This work was supported by grants from the Japanese Ministry of Education, Culture, Sports, Science and Technology (21591517 and 23591708), and the Zikei Institute of Psychiatry.

References

[1] Prusiner SB. Novel proteinaceous infectious particles cause scrapie. Science 1982;216:136–44.
[2] Prusiner SB. Molecular biology of prion diseases. Science 1991;252:1515–22.
[3] Prusiner SB. Genetic and infectious prion diseases. Arch Neurol 1993;50:1129–53 Review.
[4] Ghetti B, Piccardo P, Spillantini MG, Ichimiya Y, Porro M, Perini F, et al. Vascular variant of prion protein cerebral amyloidosis with tau-positive neurofibrillary tangles: the phenotype of the stop codon 145 mutation in PRNP. Proc Natl Acad Sci USA 1996;93:744–8.
[5] Kovács GG, Puopolo M, Ladogana A, Pocchiari M, Budka H. Genetic prion disease: the EUROCJD experience. Hum Genet 2005;118:166–74.
[6] Ladogana A, Puopolo M, Croes EA, Budka H, Jarius C. Mortality from Creutzfeldt–Jakob disease and related disorders in Europe, Australia, and Canada. Neurology 2005;64:1586–91.
[7] Nozaki I, Hamaguchi T, Sanjo N, Noguchi-Shinohara M, Sakai K, Nakamura Y, et al. Prospective 10-year surveillance of human prion diseases in Japan. Brain 2010;133:3043–57.
[8] Parchi P, Castellani R, Capellari S, Ghetti B, Young K, Chen SG, et al. Molecular basis of phenotypic variability in sporadic Creutzfeldt–Jakob disease. Ann Neurol 1996;39:767–78.
[9] Parchi P, Capellari S, Chen SG, Petersen RB, Gambetti P, Kopp N, et al. Typing prion isoforms. Nature 1997;386:232–4.
[10] Parchi P, Giese A, Capellari S, Brown P, Schurlz-Schaeffer W, Windl O, et al. Classification of sporadic Creutzfeldt–Jakob disease based on molecular and phenotypic analysis of 300 subjects. Ann Neurol 1999;46:224–33.
[11] Parchi P, Strammiello R, Notari S, Giese A, Langeveld JP, Ladogana A, et al. Incidence and spectrum of sporadic Creutzfeldt–Jakob disease variants with mixed phenotype and co-occurrence of PrPSc types: an updated classification. Acta Neuropathol 2009;118:659–71.
[12] Parchi P, Strammiello R, Giese A, Kretzschmar H. Phenotypic variability of sporadic human prion disease and its molecular basis: past, present, and future. Acta Neuropathol 2011;121:91–112.
[13] Shiga Y, Satoh K, Kitamoto T, Kanno S, Nakashima I, Sato S, et al. Two different clinical phenotypes of Creutzfeldt–Jakob disease with a M232R substitution. J Neurol 2007;254:1509–17.
[14] Chida K, Konno H, Sakuma R, Okita S, Takase S, Kitamoto T. Autopsy case of sporadic Creutzfeldt–Jakob disease with a point mutation at the codon 232 of prion protein gene. Neuropathology 1995;15(suppl):1A–6A In Japanese.
[15] Hitoshi S, Nagura H, Yamanouchi H, Kitamoto T. Double mutations at codon 180 and codon 232 of the PRNP gene in an apparently sporadic case of Creutzfeldt–Jakob disease. J Neurol Sci 1993;120:208–12.
[16] Hoque MZ, Kitamoto T, Furukawa H, Muramoto T, Tateishi J. Mutation in the prion protein gene at codon 232 in Japanese patients with Creutzfeldt–Jakob disease: a clinicopathological, immunohistochemical and transmission study. Acta Neuropathol 1996;92:441–6.
[17] Hama T, Iwasaki Y, Niwa H, Yoshida M, Hashizume Y, Kitamoto T, et al. An autopsied case of panencephalopathic-type Creutzfeldt–Jakob disease with mutation in the prion protein gene at codon 232 and type 1 prion protein. Neuropathology 2009;29:727–34.
[18] Ishida C, Endo M, Nakajima T, Fukuhara N, Makifushi T. An autopsy-proven case of Creutzfeldt–Jakob disease with a point mutation at codon 232 of the prion protein gene. Rinsho Shinkeigaku 2001;40:287 In Japanese.
[19] Okuma M, Hamada T, Okayama M, Muramoto T. Codon 232 point mutation in a patient with Creutzfeldt–Jakob disease. Dementia 1994;8:447–52 In Japanese.
[20] Shimizu T, Tanaka K, Tanahashi N, Fukuuchi Y, Kitamoto T. Creutzfeldt–Jakob disease with a point mutation at codon 232 of prion protein—a case report. Rinsho Shinkeigaku 1994;34:590–2 In Japanese.
[21] Satoh K, Muramoto T, Tanaka T, Kitamoto N, Ironside JW, Nagashima K, et al. Association of an 11–12 kDa protease-resistant prion protein fragment with subtypes of dura graft-associated Creutzfeldt–Jakob disease and other prion diseases. J Gen Virol 2003;84:2885–93.
[22] Tagawa A, Natsuno T, Suzuki M, Ono S, Shimizu N. Creutzfeldt–Jakob disease with codon 232 point mutation and showing myoclonus and PSD in the early stage. A case report. Shinkeinaika 2001;40:287 In Japanese.
[23] Capellari S, Strammiello R, Saverioni D, Kretzschmar H, Parchi P. Genetic Creutzfeldt–Jakob disease and fatal familial insomnia: insights into phenotypic variability and disease pathogenesis. Acta Neuropathol 2011;121:21–37 Epub 2010 Oct 27.
[24] Choi BY, Kim SY, Seo SY, An SS, Kim S, Park SE, et al. Mutations at codons 178, 200–129, and 232 contributed to the inherited prion diseases in Korean patients. BMC Infect Dis 2009;9:132.
[25] Iizuka T, Aihara Y, Shouji M, Hirai S. Familial Creutzfeldt–Jakob disease: a case with a point mutation at codon 232 of the PRNP gene 1994;8:453–7 In Japanese.
[26] Kannno S, Hasegawa T, Miyoshi T, Tateyama M, Shiga Y, Itoyama Y. Familial Creutzfeldt–Jakob disease with a point mutation at codon 232 showing relatively long disease duration. Rinsho Shinkeigaku 2005;45:70 In Japanese.
[27] Satoh A, Goto H, Satoh H, Tomita I, Seto M, Furukawa H, et al. A case of Creutzfeldt–Jakob disease with a point mutation at codon 232: correlation of MRI and neurologic findings. Neurology 1997;49:469–70.
[28] Saito T, Isozumi K, Komatsumoto S, Nara M, Suzuki K, Dohura K. A case of codon 232 mutation-induced Creutzfeldt–Jakob disease visualized by the MRI-FLAIR images with atypical clinical symptoms. Rinsho Shinkeigaku 2000;40:51–4 Japanese.
[29] Shimizu H, Yamada M, Matsubara N, Takano H, Umeda Y, Kawase Y, et al. Creutzfeldt–Jakob disease with an M232R substitution: report of a patient showing slowly progressive disease with abundant plaque-like PrP deposition in the cerebellum. Neuropathology 2009;29:735–43.
[30] Atarashi R, Satoh K, Sano K, Fuse T, Yamaguchi N, Ishibashi D, et al. Ultrasensitive human prion detection in cerebrospinal fluid by real-time quaking-induced conversion. Nat Med 2011;17:175–8.
[31] Kitamoto T, Shin RW, Doh-ura K, Tomokane N, Miyazono M, Muramoto T, et al. Abnormal isoform of prion proteins accumulates in the synaptic structures of the central nervous system in patients with Creutzfeldt–Jakob disease. Am J Pathol 1992;140:1285–94.
[32] Yoshioka K, Miki T, Katsuya T, Ogihara T, Sakaki Y. The 717Val-Ile substitution in amyloid precursor protein is associated with familial Alzheimer's disease regardless of ethnic groups. Biochem Biophys Res Commun 1991;178:1141–6.
[33] Kitamoto T, Ohta M, Doh-ura K, Hitoshi S, Terao Y, Tateishi J. Novel missense variants of prion protein in Creutzfeldt–Jakob disease or Gerstmann–Sträussler syndrome. Biochem Biophys Res Commun 1993;191:709–14.
[34] Kitamoto T, Mohri S, Tateishi J. Organ distribution of proteinase-resistant prion protein in humans and mice with Creutzfeldt–Jakob disease. J Gen Virol 1989;70:3371–9.
[35] Kobayashi A, Sakuma N, Matsuura Y, Mohri S, Aguzzi A, Kitamoto T. Experimental verification of a traceback phenomenon in prion infection. J Virol 2010;84:3230–8.
[36] Tateishi J, Kitamoto T, Hoque MZ, Furukawa H. Experimental transmission of Creutzfeldt–Jakob disease and related diseases to rodents. Neurology 1996;46:532–7.
[37] Zheng L, Longfei J, Jing Y, Xinqing Z, Haiqing S, Haiyan L, et al. PRNP mutations in a series of apparently sporadic neurodegenerative dementias in China. Am J Med Genet B Neuropsychiatr Genet 2008;147B:938–44.
[38] Head MW, Bunn TJ, Bishop MT, McLoughlin V, Lowrie S, McKimmie CS, et al. Prion protein heterogeneity in sporadic but not variant Creutzfeldt–Jakob disease: UK cases 1991–2002. Ann Neurol 2004;55:851–9.

[39] Puoti G, Giaccone G, Rossi G, Canciani B, Bugiani O, Tagliavini F. Sporadic Creutzfeldt–Jakob disease: co-occurrence of different types of PrP(Sc) in the same brain. Neurology 1999;53:2173–6.
[40] Cali I, Castellani R, Alshekhlee A, Cohen Y, Blevins J, Yuan J, et al. Co-existence of scrapie prion protein types 1 and 2 in sporadic Creutzfeldt–Jakob disease: its effect on the phenotype and prion-type characteristics. Brain 2009;132:2643–58 Epub 2009 Sep 4.
[41] Kobayashi A, Mizukoshi K, Iwasaki Y, Miyata H, Yoshida Y, Kitamoto T. Co-occurrence of types 1 and 2 PrP(res) in sporadic Creutzfeldt–Jakob disease MM1. Am J Pathol 2011;178:1309–15.
[42] Ghetti B, Tagliavini F, Giaccone G, Bugiani O, Frangione B, Farlow MR, et al. Familial Gerstmann–Sträussler–Scheinker disease with neurofibrillary tangles. Mol Neurobiol 1994;8:41–8 Review.
[43] Collins S, McLean CA, Masters CL. Gerstmann–Sträussler–Scheinker syndrome, fatal familial insomnia, and kuru: a review of these less common human transmissible spongiform encephalopathies. J Clin Neurosci 2001;8:387–97.
[44] Kovacs GG, Seguin J, Quadrio I, Höftberger R, Kapás I, Strreichenberger N, et al. Genetic Creutzfeldt–Jakob disease associated with the E200K mutation: characterization of a complex proteinopathy. Acta Neuropathol 2011;121:39–57.
[45] Reiniger L, Lukic A, Linehan J, Rudge P, Collinge J, Mead S, et al. Tau, prions and Aβ: the triad of neurodegeneration. Acta Neuropathol 2011;121:5–20.

OPEN ACCESS Freely available online

PLOS | ONE

Biological and Biochemical Characterization of Mice Expressing Prion Protein Devoid of the Octapeptide Repeat Region after Infection with Prions

Yoshitaka Yamaguchi[1,2], Hironori Miyata[3], Keiji Uchiyama[1], Akira Ootsuyama[4], Sachiko Inubushi[1], Tsuyoshi Mori[1], Naomi Muramatsu[1], Shigeru Katamine[2], Suehiro Sakaguchi[1,2]*

1 Division of Molecular Neurobiology, The Institute for Enzyme Research (KOSOKEN), The University of Tokushima, Tokushima, Japan, **2** Department of Molecular Microbiology and Immunology, Nagasaki University Graduate School of Biomedical Sciences, Nagasaki, Japan, **3** Animal Research Center, School of Medicine, University of Occupational and Environmental Health, Kitakyushu, Japan, **4** Department of Radiation Biology and Health, School of Medicine, University of Occupational and Environmental Health, Kitakyushu, Japan

Abstract

Accumulating lines of evidence indicate that the N-terminal domain of prion protein (PrP) is involved in prion susceptibility in mice. In this study, to investigate the role of the octapeptide repeat (OR) region alone in the N-terminal domain for the susceptibility and pathogenesis of prion disease, we intracerebrally inoculated RML scrapie prions into tg(PrPΔOR)/*Prnp*$^{0/0}$ mice, which express mouse PrP missing only the OR region on the PrP-null background. Incubation times of these mice were not extended. Protease-resistant PrPΔOR, or PrP^{Sc}ΔOR, was easily detectable but lower in the brains of these mice, compared to that in control wild-type mice. Consistently, prion titers were slightly lower and astrogliosis was milder in their brains. However, in their spinal cords, PrP^{Sc}ΔOR and prion titers were abundant and astrogliosis was as strong as in control wild-type mice. These results indicate that the role of the OR region in prion susceptibility and pathogenesis of the disease is limited. We also found that the PrP^{Sc}ΔOR, including the pre-OR residues 23–50, was unusually protease-resistant, indicating that deletion of the OR region could cause structural changes to the pre-OR region upon prion infection, leading to formation of a protease-resistant structure for the pre-OR region.

Citation: Yamaguchi Y, Miyata H, Uchiyama K, Ootsuyama A, Inubushi S, et al. (2012) Biological and Biochemical Characterization of Mice Expressing Prion Protein Devoid of the Octapeptide Repeat Region after Infection with Prions. PLoS ONE 7(8): e43540. doi:10.1371/journal.pone.0043540

Editor: Jiyan Ma, Ohio State University, United States of America

Received February 23, 2012; **Accepted** July 23, 2012; **Published** August 21, 2012

Copyright: © 2012 Yamaguchi et al. This is an open-access article distributed under the terms of the Creative Commons Attribution License, which permits unrestricted use, distribution, and reproduction in any medium, provided the original author and source are credited.

Funding: This work was partly supported by a Grant-in-Aid from the bovine spongiform encephalopathy (BSE) and other Prion Disease Control Project of the Ministry of Agriculture, Forestry and Fisheries of Japan, and Grants-in-Aid from the Research Committee of Prion Disease and Slow Virus infection, the Ministry of Health, Labour and Welfare of Japan. H.M. is partly supported by a Cooperative Research Grant of the Institute for Enzyme Research, the University of Tokushima. The funders had no role in study design, data collection and analysis, decision to publish, or preparation of the manuscript. No additional external funding was received for this study.

Competing Interests: The authors have declared that no competing interests exist.

* E-mail: sakaguch@ier.tokushima-u.ac.jp

Introduction

Transmissible spongiform encephalopathies or prion diseases, which include Creutzfeldt-Jakob disease in humans and scrapie and bovine spongiform encephalopathy in animals, are neurodegenerative disorders caused by prions [1,2]. Prions consist mainly of the abnormally folded, proteinase K (PK)-resistant isoform of prion protein, designated PrP^{Sc} [3]. Structural conversion of the normal cellular isoform, designated PrP^{C}, into PrP^{Sc} is a key event in prion propagation. Indeed, mice devoid of PrP^{C} (*Prnp*$^{0/0}$) are resistant to the disease without PrP^{Sc} accumulation and prion propagation in the brain, even after inoculation with prions [4,5,6,7]. However, the exact conversion mechanism remains largely unknown.

PrP^{C} is a glycoprotein tethered to the outer cell membrane via a glycosylphosphatidylinositol anchor moiety and expressed most abundantly in the brain, particularly by neurons [8]. Reduction in susceptibility to RML scrapie prions was reported in tg(PrPΔ32–93)/*Prnp*$^{0/0}$ and tg(PrPΔ23–88)/*Prnp*$^{0/0}$ mice, which express mouse (mo) PrP lacking residues 32–93 or 23–88 on the *Prnp*$^{0/0}$ background, respectively [9,10]. The incubation times of these mice were accordingly extended [9,10]. The incubation times of experimental prion diseases in mice are usually inversely correlated to the expression level of PrP^{C} in the brain. Indeed, tg(moPrP)/*Prnp*$^{0/0}$ mice, which express mouse wild-type PrP^{C} in the brains at 8 fold higher levels than control wild-type mice, showed a shorter incubation time of 50±2 days post-inoculation (dpi) with RML prions, while the wild-type mice became sick at 127±1 dpi [10,11]. Tg(PrPΔ23–88)/*Prnp*$^{0/0}$ mice were shown to express PrPΔ23–88 in their brains two fold higher than moPrP^{C} in tg(moPrP)/*Prnp*$^{0/0}$ mice [10]. However, tg(PrPΔ23–88)/*Prnp*$^{0/0}$ mice developed the disease with a longer incubation time of 161±4 dpi than tg(moPrP)/*Prnp*$^{0/0}$ mice with 50±2 dpi [10]. Tg(PrPΔ32–93)/*Prnp*$^{0/0}$ mice also developed the disease with longer incubation times of 232 to 313 dpi than control wild-type mice with 158±11 dpi, although tg(PrPΔ32–93)/*Prnp*$^{0/0}$ mice expressed PrPΔ32–93 in the brains 4 fold higher than PrP^{C} in the control mice [9]. These results indicate that the N-terminal residues of PrP affect susceptibility to RML prions in mice. It was also reported that the MHM2(Δ23–88) molecule, a mouse-hamster chimeric PrP deletion mutant carrying hamster PrP-derived methionine residues at 108 and 111 substituted for leucine

and valine residues in mouse PrPΔ23–88, completely failed to restore susceptibility to RML prions in *Prnp*$^{0/0}$ mice [10,11]. These results indicate that the chimeric region, corresponding to residues 108 through 111, also influences the susceptibility to RML prions in mice.

The so-called octapeptide repeat (OR) region, which comprises 5 copies of an octapeptide sequence, is located in the unstructured N-terminal domain of PrP. PrPΔ32–93 lacks the entire OR region (residues 51–90) and most of the OR region is missing in PrPΔ23–88. It is thus suggested that the OR region might be involved in the susceptibility to RML prions in mice. However, PrPΔ32–93 and PrPΔ23–88 lack not only the OR region but also other regions. Therefore, it still remains unclear whether the decreased susceptibility in tg(PrPΔ32–93)/*Prnp*$^{0/0}$ and tg(PrPΔ23–88)/*Prnp*$^{0/0}$ mice could be due to the deletion of the OR region either alone or together with other regions.

Unusual phenotypes were reported in infected tg(PrPΔ32–93)/*Prnp*$^{0/0}$ mice. PrP^{Sc}Δ32–93 was hardly detectable in the brains of terminally ill tg(PrPΔ32–93)/*Prnp*$^{0/0}$ mice [9]. Prion infectivity was accordingly reduced and disease-specific vaculoation and astrogliosis were undetectable in their brains [9]. However, in the spinal cord, prion infectivity and the pathological changes were similarly observed between tg(PrPΔ32–93)/*Prnp*$^{0/0}$ and control mice [9]. Infected tg(PrPΔ32–93)/*Prnp*$^{0/0}$ mice also displayed the unusual symptom of foreleg paresis [9]. In contrast, no such unusual phenotypes were detected in infected tg(PrPΔ23–88)/*Prnp*$^{0/0}$ mice. Residues 89–93 are missing in PrPΔ32–93, but not in PrPΔ23–88. Therefore, deletion of these residues might be involved in development of the unusual phenotypes, as observed in infected tg(PrPΔ32–93)/*Prnp*$^{0/0}$ mice. However, this possibility still remains to be clarified.

We previously established a tg mouse line, designated tg(PrPΔOR)/*Prnp*$^{0/0}$, which expresses mouse PrP with a deletion of the OR region alone on the *Prnp*$^{0/0}$ background [12]. In the present study, to investigate the role of the OR region alone in prion susceptibility and the pathogenesis of prion disease, we intracerebrally inoculated RML prions into tg(PrPΔOR)/*Prnp*$^{0/0}$ mice.

Materials and Methods

Ethics Statement

The Ethics Committee of Animal Care and Experimentation of University of Occupational and Environmental Health, Kitakyushu, Japan approved this study (approval number AE-080-13). Animals were cared for in accordance with The Guiding Principle for Animal Care and Experimentation of University of Occupational and Environmental Health and Japanese Law for Animal Welfare and Care.

Animals

C57BL/6 mice were purchased from CLEA Japan, Tokyo, Japan and ddY mice were from Kyudo, Tosu, Japan. ddY mice are outbred albino mice maintained in a closed colony. Tg(PrPΔOR)/*Prnp*$^{0/0}$ mice with the C57BL/6×129Sv×FVB mixed background were produced elsewhere [12]. In this study, tg(PrPΔOR)/*Prnp*$^{0/0}$ mice (C57BL/6×129Sv×FVB) were crossed at least more than twice with Zrch I *Prnp*$^{0/0}$ mice, which had been backcrossed to C57BL/6 mice more than 9 times.

Prion Inoculation

Brains were removed from terminally ill wild-type C57BL/6 mice infected with RML prions. A single brain was homogenized (10%, w/v) in phosphate-buffered saline (PBS) by passing it through 18 to 26 gauge needles and then diluted to 1% with PBS. Four to five week-old mice were intracerebrally inoculated with a 20 μl-aliquot of the homogenates.

Western Blotting

Tissue homogenates (10%, w/v) were prepared in lysis buffer containing 150 mM NaCl, 50 mM Tris-HCl (pH 7.5), 0.5% Triton X-100, 0.5% sodium deoxycholate, 1 mM EDTA, and protease inhibitor mixture (Nakalai Tesque Co., Kyoto, Japan) by passing them through 18 to 26 gauge needles and centrifugation at low speed to remove debris. Protein concentrations of the resulting supernatant were determined using the BCA protein assay kit (Pierce, Rockford, USA.). Total proteins treated with or without PK (Wako Pure Chemical Industries, Ltd., Osaka, Japan) at 20 μg/ml for 30 min at 37°C were electrophoresed through a 12% SDS-polyacrylamide gel and electrically transferred to an Immobilon-P PVDF membrane (Millipore Corp., MA, USA). The membrane was immersed in 5% non-fat dry milk-containing TBST (0.1% Tween-20, 100 mM NaCl, 10 mM Tris-HCl, pH 7.6) for 1 h at room temperature (RT), and incubated with SAF32 and SAF61 mouse monoclonal antibodies (SPI-BIO, Montigny le Bretonneux, France), M20 goat polyclonal antibodies (Santa Cruz Biotechnology, Inc., Santa Cruz, CA), IBL-N rabbit polyclonal antibodies (Immuno Biological Laboratories, Gunma, Japan), 3F4 monoclonal antibody (Signet Laboratories Inc., Dedham, MA), anti-human glial fibrillary acidic protein (GFAP) IgG rabbit polyclonal antibodies (SHIMA Laboratories Co., LTD, Tokyo, Japan) or anti-β-actin monoclonal antibody (Sigma-Aldrich, Inc., St. Louis, MO) for 2 h at RT or overnight at 4°C in 1% non-fat dry milk-containing TBST. The membrane was washed in TBST for 15 min once and for 5 min three times. Signals were visualized using horseradish peroxidase (HRP)-conjugated anti-mouse IgG antibodies (Amersham Biosciences Inc., Piscataway, NJ), anti-rabbit IgG antibodies (Amersham Biosciences Inc.), and anti-goat IgG antibodies (CHEMICON International, Inc., Temecula, CA) and Immobilon^{TM} Western Chemiluminesent HRP substrate (Millipore) and detected using a chemiluminescence image analyzer, LAS-4000 mini (Fujifilm Co., Tokyo, Japan).

Immunohistochemistry

Paraffin embedded samples were sectioned, deparaffinized, rehydrated and treated with L.A.B. Solution (Polysciences, Inc., U.S.A.) for 10 min. Nonspecific endogenous peroxidase activity was quenched by incubating the specimens with 3% H_2O_2 for 10 min and then the specimens were blocked with 5% normal rabbit serum for 10 min at RT. For detection of PrP^{Sc} or PrP^{Sc}ΔOR, the specimens were treated with formic acid for 1 min before the blocking step. The specimens were then incubated with 1/500 polyclonal rabbit anti-GFAP antibodies (DAKO Cytomation, Denmark) or 1/100 polyclonal rabbit IBL-N anti-PrP antibodies (Immuno Biological Laboratories) for 2 h at RT. After washing in PBS, the specimens were incubated with HRP-labeled polymer anti-rabbit (EnVision^{TM} System, DAKO Cytomation, Denmark) for 1 h at RT, washed in PBS, and then visualized using the avidin-biotin complex method (Vector Labs, U.S.A.). The nuclei were counterstained with Mayer's hematoxylin.

PNGase F Digestion

PNGase F digestion was performed according to the manufacturer's protocol (New England Biolabs, Inc., Ipswich, MA). Briefly, the PK-treated homogenates were denatured by boiling for 10 min in the presence of 0.5% SDS and 1% mercaptoethanol

and then treated with PNGase F (500 units/L) in 1% Nonidet P-40 and 0.05 M sodium phosphate (pH 7.5) for 60 min at 37°C.

Standard Curve and Prion Titer Determination

To create a standard curve between prion titers and incubation times, 10% (w/v) brain homogenate of RML-infected ddY mice were serially diluted 10-fold with PBS, ranging from 10^{-1} to 10^{-10} in PBS, and a 20 µl-aliquot of each dilution was intracerebrally inoculated into ddY mice aged 4–5 weeks. The mice were observed until 1 year after inoculation. The ID_{50}/gram of the tissue was determined according to the method of Reed and Muench and then a standard curve was created. Prions titers (ID_{50}/g) in tissues of interest were determined as follows: A 20 µl-aliquot of the tissue homogenates was intracerebrally inoculated into 5 or 6 ddY mice aged 4–5 weeks and their incubation times were determined. Thereafter, prion titers in the homogenates were calculated using the standard curve.

Expression Vectors

To construct an expression vector encoding mouse PrP tagged with the 3F4 epitope designated moPrP(3F4), the 5′ fragment of mouse PrP cDNA was amplified by polymerase chain reaction (PCR) using a mouse PrP cDNA as a template with a BamHI-PrP(ATG)-S sense primer (Table S1) and a moPrP-3F4 anti-sense primer (Table S1). Then, full-length PrP cDNA was amplified by PCR using a mouse PrP cDNA as a template with the amplified 5′ fragment as a sense primer and a PrP(stop)-XbaI-AS anti-sense primer (Table S1). After sequence confirmation, the amplified fragment was inserted into *Bam*H I/*Xba* I-digested pcDNA3.1(+) (Invitrogen, Carlsbad, CA), resulting in pcDNA3.1-moPrP(3F4).

To construct an expression vector encoding the 3F4-tagged mouse PrP with a deletion of residues 32–88, designated moPrP(3F4) Δ32–88, the 5′ fragment of moPrP(3F4) Δ32–88 cDNA was amplified by PCR using pcDNA3.1-moPrP(3F4) as a template with a BamHI-PrP(ATG)-S sense primer and a PrP32–88 anti-sense primer (Table S1). Then, full-length moPrP(3F4) Δ32–88 cDNA was amplified by PCR using pcDNA3.1-moPrP(3F4) as a template with the amplified 5′ fragment as a sense primer and a PrP(stop)-XbaI-AS anti-sense primer. After sequence confirmation, the amplified fragment was inserted into *Bam*H I/*Xba* I-digested pcDNA3.1(+) (Invitrogen, Carlsbad, CA), resulting in pcDNA3.1-moPrP(3F4)32–88.

To construct expression vectors encoding moPrP(3F4) Δ32–88(3K3A), moPrP(3F4) Δ32–88(K23A), moPrP(3F4) Δ32–88(K24A), moPrP(3F4) Δ32–88(K27A), moPrP(3F4) Δ32–88(K23,24A), moPrP(3F4) Δ32–88(K23,27A), moPrP(3F4) Δ32–88(K24,27A), moPrP(3F4) Δ32–88(3K3R), moPrP(3F4) Δ32–88(2P2A), moPrP(3F4) Δ32–88(2P2G) and moPrP(3F4) Δ32–88(2P2W), the 5′ fragment of the moPrP(3F4) Δ32–88 vector was amplified by PCR using a vector-derived T7 sense primer (Table S1) and an antisense primer (Table S1) of PrP(3K3A)-AS, PrP(K23A)-AS, PrP(K24A)-AS, PrP(K27A)-AS, PrP(K23/24A)-AS, PrP(K23/27A)-AS, PrP(K24/27A)-AS, PrP(3K3R)-AS, PrP(2P2A)-AS, PrP(2P2G)-AS or PrP(2P2W)-AS, respectively. The amplified fragments were then used as sense primers for amplification of full-length cDNAs encoding each mutant PrP with a vector-derived BGH reverse primer (Table S1) as an antisense primer using the moPrP(3F4) Δ32–88 vector as a template. After sequence confirmation, each amplified fragment was inserted into *Bam*H I/*Xba* I-digested pcDNA3.1(+) (Invitrogen).

Transfection

Mouse neuroblastoma N2a cells persistently infected with 22L prions, designated N2aC24L1-3 [13], were transiently transfected with expression vectors using Lipofectamine 2000 reagent (Invitrogen). The cells were lysed in a buffer (150 mM NaCl, 0.5% Triton X-100, 0.5% sodium deoxycholate, 50 mM Tris-HCl, pH 7.5) 2 days after transfection and subjected to Western blotting.

Statistical Analysis

Log-rank test was used for analysis of the incubation times of infected mice.

Results

Incubation Times and Foreleg Paresis in tg(PrPΔOR)/*Prnp*$^{0/0}$ Mice after Infection with RML Prions

We intracerebrally inoculated RML prions into tg(PrPΔOR)/*Prnp*$^{0/0}$ mice and control C57BL/6 wild-type mice. Uninfected tg(PrPΔOR)/*Prnp*$^{0/0}$ mice remained healthy for more than 500 days. Wild-type mice developed disease-specific symptoms, such as weight loss, decreased locomotive activity, ruffled hair coat and hunched back, at 165±4 days post-inoculation (dpi) (Table 1). Tg(PrPΔOR)/*Prnp*$^{0/0}$ mice succumbed to the disease with slightly shorter incubation times of 147±9 dpi (Table 1). This is probably due to higher expression of PrPΔOR in the brains of tg(PrPΔOR)/*Prnp*$^{0/0}$ mice than in that of PrP^{C} in wild-type mice. PrPΔOR was detected in the brain and spinal cord about 2–3 fold more than PrP^{C} in wild-type mice on Western blotting using SAF61 anti-PrP antibodies, which recognize residues 142–160 (human PrP numbering) (Fig. 1). Lack of the OR region in PrPΔOR was confirmed by Western blotting using SAF32 anti-OR region antibody (Fig. 1). Tg(PrPΔOR)/*Prnp*$^{0/0}$ mice also displayed the additional unusual symptom of foreleg paresis at early stages of the disease.

Astrogliosis in tg(PrPΔOR)/*Prnp*$^{0/0}$ Mice Infected with RML Prions

We investigated brain and cervical cord sections from terminally ill tg(PrPΔOR)/*Prnp*$^{0/0}$ and wild-type mice for astrogliosis, a pathological hallmark of prion diseases, by immunohistochemical analysis using anti-GFAP antibodies. Astrogliosis was stronger in the brain and cervical cord sections from infected tg(PrPΔOR)/*Prnp*$^{0/0}$ and wild-type mice, compared to that in uninfected tg(PrPΔOR)/*Prnp*$^{0/0}$ and wild-type mice (Fig. 2, A and B). However, brain astrogliosis in infected tg(PrPΔOR)/*Prnp*$^{0/0}$ mice was slightly milder than in infected wild-type mice (Fig. 2A). In contrast, in the cervical cord sections, astrogliosis was as strong in infected tg(PrPΔOR)/*Prnp*$^{0/0}$ mice, as in infected wild-type mice (Fig. 2B). Western blotting showed consistent results. Compared to the GFAP expression in infected wild-type mice, it was mildly decreased in the brains of infected tg(PrPΔOR)/*Prnp*$^{0/0}$ mice, but not in their spinal cords (Fig. 2, C and D). We also investigated the brain sections of terminally ill tg(PrPΔOR)/*Prnp*$^{0/0}$ and wild-type mice for spongiosis. Vacuoles were similarly observed in the brains of both types of mice, scant in the cerebral cortex (Fig. S1A) but common in the hippocampus (Fig. S1B) and cerebellum (Fig. S1C). The brain sections were further immunohistochemically stained for abnormal PrP isoforms, PrP^{Sc} and PrP^{Sc}ΔOR, with IBL-N anti-PrP antibodies, which were raised against the N-terminal residues 24–37, after treatment with formic acid. The immunoreactive signals were strong in the brains of both types of infected mice, compared to those in control uninfected mice, and were similarly distributed in the brains of both types of infected mice (Fig. S2).

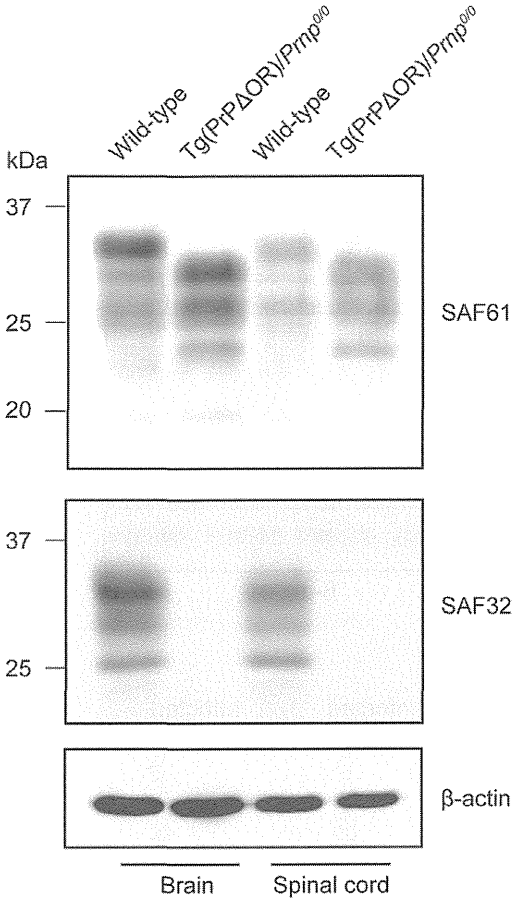

Figure 1. Overexpression of PrPΔOR in the brains and spinal cords of tg(PrPΔOR)/*Prnp*$^{0/0}$ mice. The brain and spinal cord homogenates from tg(PrPΔOR)/*Prnp*$^{0/0}$ mice and wild-type mice were subjected to Western blotting with SAF61 or SAF32 anti-PrP antibodies. The expression of β-actin was detected in these homogenates as an internal control.
doi:10.1371/journal.pone.0043540.g001

PK-resistant PrP, or PrP^{Sc}ΔOR, in tg(PrPΔOR)/*Prnp*$^{0/0}$ Mice Infected with RML Prions

We investigated the brains and spinal cords of terminally ill tg(PrPΔOR)/*Prnp*$^{0/0}$ and wild-type mice for PK-resistant isoforms, PrP^{Sc}ΔOR and wild-type PrP^{Sc}, respectively, using Western blotting with SAF61 antibodies. PrP^{Sc}ΔOR was easily detectable in the brains and spinal cords of two individual tg(PrPΔOR)/*Prnp*$^{0/0}$ mice (Fig. 3, A and B). However, compared to wild-type PrP^{Sc} in infected wild-type mice, a reduced amount of PrP^{Sc}ΔOR was detected in the brains of infected tg(PrPΔOR)/*Prnp*$^{0/0}$ mice (Fig. 3A). Western blotting of the brains showed that total PrPs were more abundant in infected wild-type mice than in infected tg(PrPΔOR)/*Prnp*$^{0/0}$ mice (Fig. 3A), despite PrPΔOR being expressed in the brains of uninfected tg(PrPΔOR)/*Prnp*$^{0/0}$ mice more than PrP^{C} in uninfected wild-type mice (Fig. 1A). This is probably due to different amounts of wild-type PrP^{Sc} and PrP^{Sc}ΔOR accumulating in the brains. In the spinal cords, the amount of PrP^{Sc}ΔOR in infected tg(PrPΔOR)/*Prnp*$^{0/0}$ mice was similar to that of wild-type PrP^{Sc} in infected wild-type mice (Fig. 3B).

Prion Propagation in tg(PrPΔOR)/*Prnp*$^{0/0}$ Mice Infected with RML Prions

We also determined prion titers (LD_{50}/gram of tissue) in the brains and spinal cords of terminally ill tg(PrPΔOR)/*Prnp*$^{0/0}$ and wild-type mice. To do this, we first created a standard curve between prion titers and incubation times by intracerebral inoculation of serially diluted brain homogenates of RML prion-affected mice into indicator mice. The mortalities and incubation times of the indicator mice are shown in Table 2. According to the method of Reed and Muench [14], prion titers of the homogenate were calculated as $10^{8.5}$ LD_{50}/g. The standard curve was given by $Log_{10}(LD_{50}/g) = 14.08 - 0.05X$, where X is incubation time (days), $131 < x < 215$. We thereafter intracerebrally inoculated the homogenates of 2 pooled brains and 2 pooled spinal cords from the terminally ill wild-type and tg(PrPΔOR)/*Prnp*$^{0/0}$ mice into indicator mice. The brain and spinal cord used were from the same mouse. The inoculation of wild-type brain homogenate caused the disease in indicator mice at 112±1 dpi, whereupon prion titers in the homogenate were calculated as >7.5 Log(LD_{50}/g) (Table 3). However, after inoculation with tg(PrPΔOR)/*Prnp*$^{0/0}$ brain homogenate, the indicator mice succumbed to the disease with significantly longer incubation times of 150±8 dpi (Log-rank test, $p = 0.0455$), indicating that prion titers in the brains of terminally ill tg(PrPΔOR)/*Prnp*$^{0/0}$ mice were 6.7 Log(LD_{50}/g) (Table 2). In contrast, in the spinal cords of infected tg(PrPΔOR)/*Prnp*$^{0/0}$ mice, prion titers were not reduced (Table 3). The spinal cord homogenates from terminally ill wild-type and tg(PrPΔOR)/*Prnp*$^{0/0}$ mice rendered the indicator mice ill at 159±8 and 142±13 dpi (Log-rank test, $p = 0.3321$), with prion titers in the homogenates being calculated as 6.3 and 7.0 Log(LD_{50}/g), respectively (Table 3).

The Pre-OR Region is Unusually PK-resistant in PrP^{Sc}ΔOR

We recognized that the PK-resistant fragments of PrP^{Sc}ΔOR in the brains and spinal cords appeared to migrate slightly slower than those of wild-type PrP^{Sc} on Western blotting (Fig. 3, A and B). This suggests that the PK-resistant core of PrP^{Sc}ΔOR is higher in molecular weight than that of wild-type PrP^{Sc}. To confirm this, we treated the PK-digested brain homogenates from terminally ill tg(PrPΔOR)/*Prnp*$^{0/0}$ and wild-type mice with PNGase F before subjecting them to Western blotting. The molecular size of the deglycosylated PK-resistant fragment of PrP^{Sc}ΔOR was clearly higher than that of wild-type PrP^{Sc} (Fig. 4A). We also performed Western blotting of the brain homogenates with IBL-N antibodies raised against the N-

Table 1. Incubation times in tg(PrPΔOR)/*Prnp*$^{0/0}$ and wild-type mice after infection with RML prions.

Mouse line	Incubation times (Mean±SD, days)	Diseased/Inoculated
Wild-type (C57BL/6)	165±4	10/10
Tg(PrPΔOR)/*Prnp0/0*	147±9	8/8

doi:10.1371/journal.pone.0043540.t001

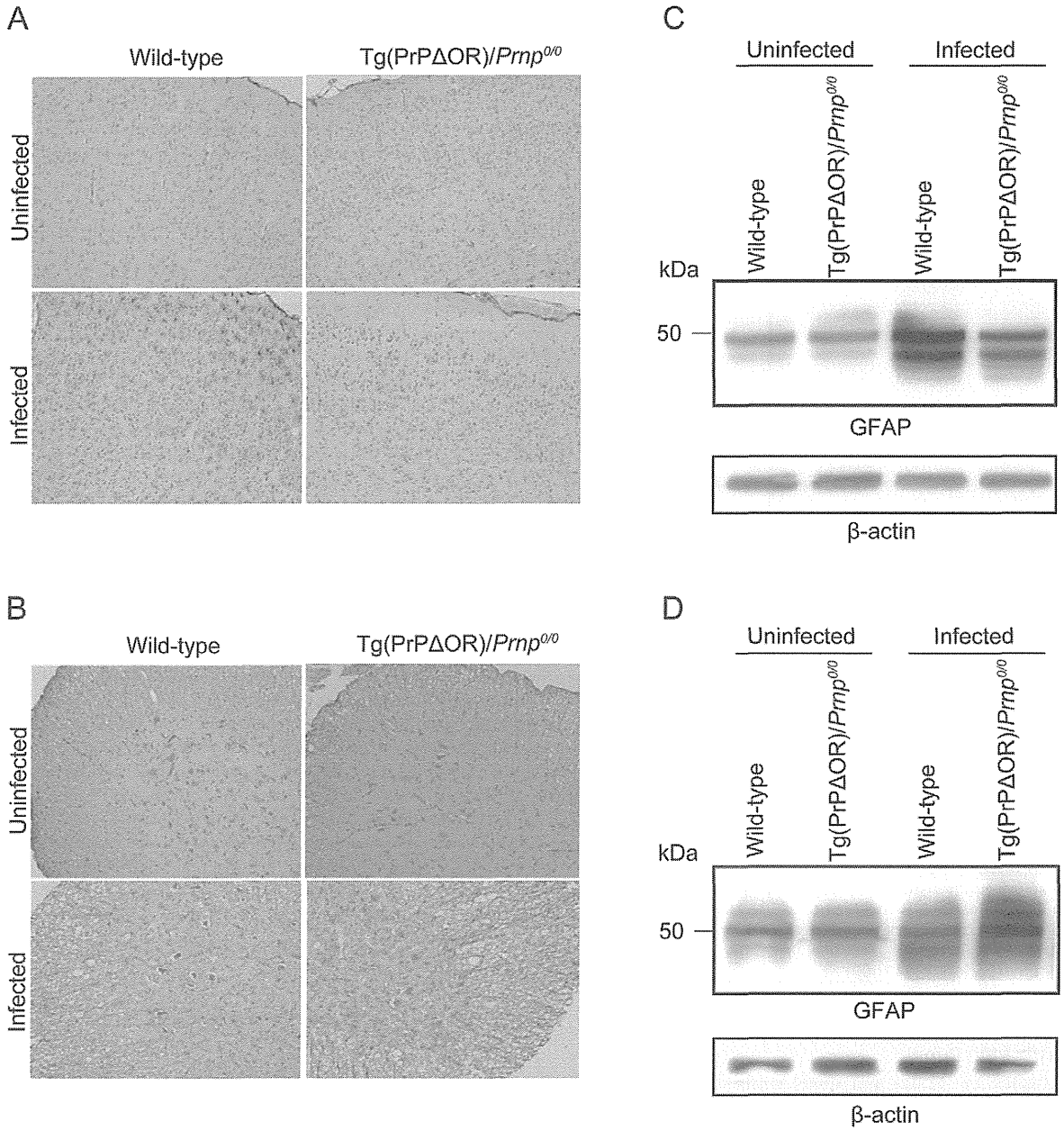

Figure 2. Astrogliosis in the brains and cervical cords of tg(PrPΔOR)/*Prnp*$^{0/0}$ mice infected with RML prions. The cerebral cortices (A) and cervical cords (B) of uninfected or terminally ill wild-type and tg(PrPΔOR)/*Prnp*$^{0/0}$ mice were immunohistochemically stained with anti-GFAP antibodies. The signals were milder in the brains of terminally ill tg(PrPΔOR)/*Prnp*$^{0/0}$ mice, compared to those in control wild-type mice. No decrease in the signals was observed in the cervical cords of terminally ill tg(PrPΔOR)/*Prnp*$^{0/0}$ mice. Immunoblots of the homogenates of brains (C) and spinal cords (D) of uninfected and terminally ill wild-type and tg(PrPΔOR)/*Prnp*$^{0/0}$ mice using anti-GFAP antibodies are shown. Terminally ill tg(PrPΔOR)/*Prnp*$^{0/0}$ mice expressed GFAP in their brains less than control wild-type mice. No reduction in the GFAP expression was detected in the spinal cords of terminally ill tg(PrPΔOR)/*Prnp*$^{0/0}$ mice.
doi:10.1371/journal.pone.0043540.g002

terminal residues 24–37 of PrP. The antibody reacted with the PK-resistant fragments from PrP^{Sc}ΔOR but not from wild-type PrP^{Sc} (Fig. 4B). We detected no PK-resistant fragments with molecular size >2 kDa in the brains of terminally ill wild-type mice on Western blotting using IBL-N antibodies (data not shown). Taken together, these results suggest that the entire PrP^{Sc}ΔOR, including the pre-OR residues is PK-resistant, while only the C-terminal part is PK-resistant in wild-type PrP^{Sc}.

Deletion of OR Residues 51–88 Renders the Pre-OR Residues PK-resistant in Prion-infected N2a Cells

Since PrPΔ32–93 in tg(PrPΔ32–93)/*Prnp*$^{0/0}$ mice lacks the entire OR region [9], we asked whether or not the remaining pre-OR residues could become PK-resistant upon conversion. In addition, since PrPΔ23–88 in tg(PrPΔ23–88)/*Prnp*$^{0/0}$ mice has 2 residues intact in the OR region [10], we also asked whether the 2 remaining OR residues in PrPΔ23–88 could potentially block the

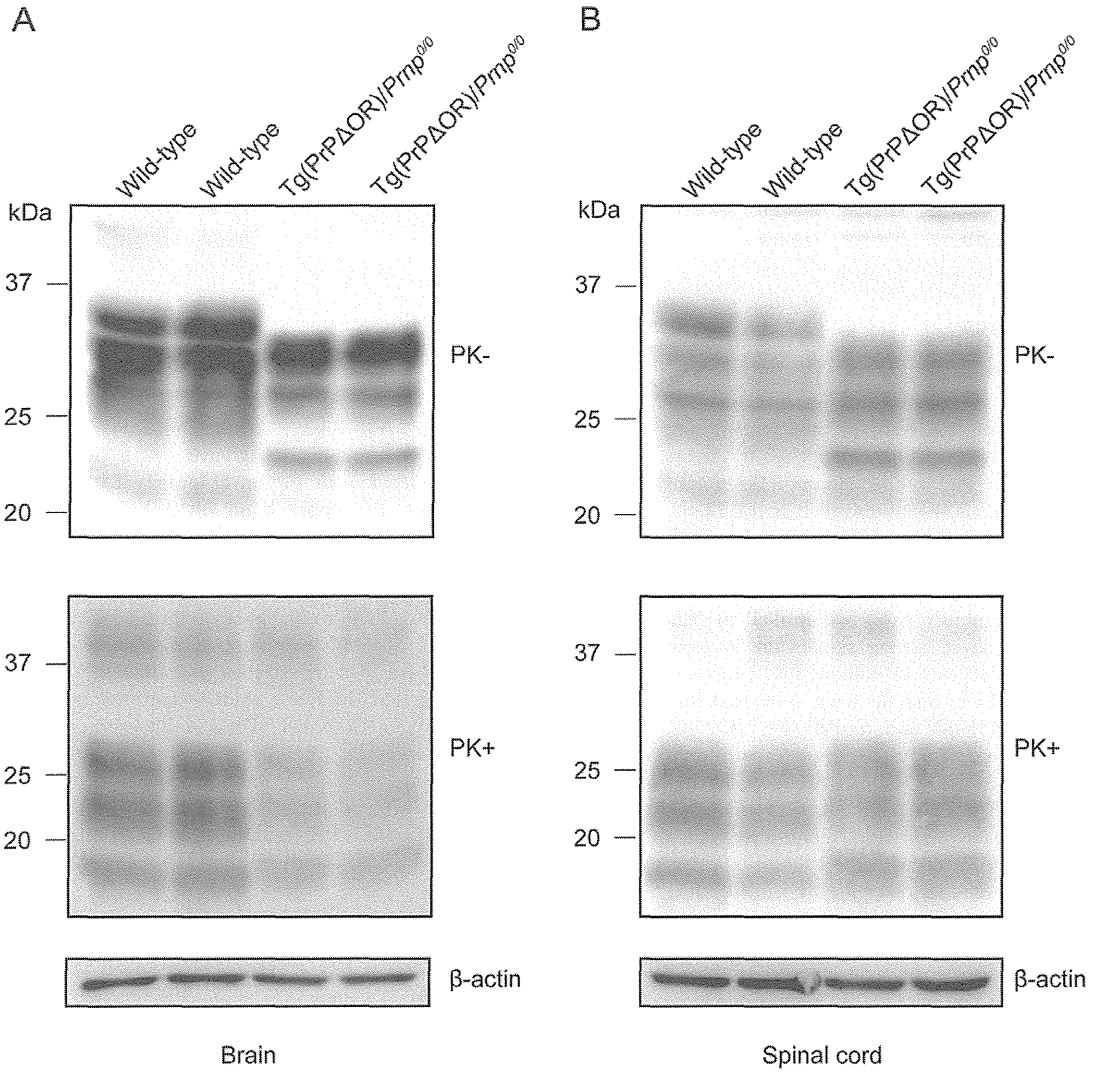

Figure 3. PK-resistant PrP accumulated in the brains and spinal cords of terminally ill tg(PrPΔOR)/*Prnp*$^{0/0}$ mice. Immunoblots of the two PK-treated individual brains (A) and spinal cords (B) from terminally ill wild-type and tg(PrPΔOR)/*Prnp*$^{0/0}$ mice using SAF61 anti-PrP antibodies.
doi:10.1371/journal.pone.0043540.g003

Table 2. Incidence rate and incubation times in wild-type ddY indicator mice inoculated with serial 10-fold dilutions of RML prions.

Dilution of inoculum (log_{10} dilution)	Incidence rate (Symptomatic mice/Total mice)	Incubation times (Mean±SD, days)
−1	6/6	131±3
−2	6/6	158±3
−3	6/6	177±6
−4	6/6	190±6
−5	6/6	215±33
−6	2/6	243, 285
−7	1/6	229
−8	0/6	
−9	0/6	
−10	0/6	

doi:10.1371/journal.pone.0043540.t002

Table 3. Prion titers in the brains and spinal cords of terminally ill tg(PrPΔOR)/*Prnp*$^{0/0}$ and wild-type mice inoculated with RML prions.

Inoculum	Donor mouse line	Incubation times (mean ±SD, days) in indicator mice	Log-rank test *p* value	Incidence rate in indicator mice (Symptomatic/Total)	Prion titers (Log_{10}/gram of tissue)
Brains (2 pooled)	Wild-type	112±1		6/6	>7.5
	Tg(PrPΔOR)/*Prnp0/0*	150±8	0.046	6/6	6.6
Spinal cords (2 pooled)	Wild-type	159±8		5/5	6.3
	Tg(PrPΔOR)/*Prnp0/0*	142±13	0.332	6/6	7.0

doi:10.1371/journal.pone.0043540.t003

pre-OR residues from becoming PK-resistant upon conversion. To address these questions, we constructed expression vectors encoding the 3F4-tagged mouse PrP with or without a deletion of residues 32–88, designated moPrP(3F4) and moPrP(3F4) Δ32–88, respectively (Fig. 5A), and transiently transfected them into 22L prion-infected N2a cells, designated N2aC24L1-3 cells. Using 3F4 anti-PrP antibodies, moPrP(3F4) and moPrP(3F4) Δ32–88 can be distinguished from the endogenously expressed moPrP in N2a cells. The 3F4 antibody displayed strong signals on Western blotting of the cell lysates treated with or without PK, indicating that moPrP(3F4) and moPrP(3F4) Δ32–88 were converted into PK-resistant isoforms, moPrP(3F4)^{Sc} and moPrP(3F4)^{Sc}Δ32–88, respectively (Fig. 5B). Each band of non-glycosylated and mono-glycosylated moPrP(3F4)^{Sc} was single (Fig. 5B). However, they were doublet in moPrP(3F4)^{Sc}Δ32–88 (Fig. 5B), suggesting that each upper band of non-glycosylated and mono-glycosylated signals could be moPrP(3F4)^{Sc}Δ32–88 with the PK-resistant pre-OR region. Indeed, IBL-N antibodies reacted only with the PK-resistant fragments from moPrP(3F4)^{Sc}Δ32–88, but not from moPrP(3F4)^{Sc} (Fig. 5C). The non-glycosylated band of moPrP(3F4)^{Sc}Δ23–88 seemed smaller in molecular size to that of PrP^{Sc}ΔOR on Western blotting (compare Fig. 4, A and B to Fig. 5, B and C). The non-glycosylated band of PrP^{Sc}ΔOR was detected around 20 kDa while that of moPrP(3F4)^{Sc}Δ23–88 was around 17–18 kDa (Fig. 5, B and C). This is probably because the deletion in moPrP(3F4) Δ23–88 is larger than in PrPΔOR. Taken together, these results clearly indicate that the entire pre-OR region of some moPrP(3F4)^{Sc}Δ32–88 molecules are PK-resistant, and that the remaining 2 OR residues have no potential to block the pre-OR residues from becoming PK-resistant.

Lysine Residues are Important for the Pre-OR Residues of moPrP(3F4) Δ32–88 to form a PK-resistant Structure upon Conversion in Prion-infected N2a Cells

The pre-OR residues 23–31 include a very conserved positively charged region consisting of 3 lysine residues and 2 proline residues (Fig. 6A). To gain insights into the mechanism for the pre-OR residues 23–31 to be converted into a PK-resistant structure, we also constructed expression vectors encoding moPrP(3F4) Δ32–88 with a substitution of all the lysine residues or all the proline residues by alanine residues, designated moPrP(3F4) Δ32–88(3K3A) and moPrP(3F4) Δ32–88(2P2A), respectively (Fig. 6A). Western blotting with 3F4 anti-PrP antibodies revealed that both mutant proteins were converted into PK-resistant isoforms in N2aC24L1-3 cells (Fig. 6B). Non-glycosylated and mono-glycosylated bands of moPrP(3F4)^{Sc}Δ32–88(2P2A) and moPrP(3F4)^{Sc}Δ32–88(3K3A) were doublet (Fig. 6B). However, the upper band of the doublet was different in molecular size between moPrP(3F4)^{Sc}Δ32–88(2P2A) and moPrP(3F4)^{Sc}Δ32–88(3K3A). MoPrP(3F4)^{Sc}Δ32–88(2P2A) gave rise to the upper band with similar molecular size to that of moPrP(3F4)^{Sc}Δ32–88 (Fig. 6B). In contrast, the upper band of moPrP(3F4)^{Sc}Δ32–88(3K3A) was reduced in its molecular size and migrated very closely to the lower band (Fig. 6B). The upper band of the doublet is indicative of the PK-resistant PrP molecule with the PK-resistant pre-OR residues. Thus, these results indicate that, while the pre-OR residues 23–31 are PK-resistant in moPrP(3F4)^{Sc}Δ32–88(2P2A), most of them are PK-sensitive in moPrP(3F4)^{Sc}Δ32–88(3K3A), suggesting that the lysine residues play an important role for the pre-OR region of moPrP(3F4) Δ32–88 to become PK-resistant in N2aC24L1-3 cells. The substitution disrupted the IBL-N epitope, resulting in loss of the immunoreativities with IBL-N antibodies (Fig. 6C). Therefore, IBL-N antibodies were not available to detect the PK-resistant pre-OR region of moPrP(3F4)^{Sc}Δ32–88(3K3A) and moPrP(3F4)^{Sc}Δ32–88(2P2A) (Fig. 6C).

The proline residues in moPrP(3F4) Δ32–88 were further substituted for tryptophan or glycine residues in moPrP(3F4) Δ32–88(2P2W) and moPrP(3F4) Δ32–88(2P2G), respectively (Fig. 7A). Western blotting with 3F4 antibodies showed that these mutant proteins were converted into PK-resistant isoforms, moPrP(3F4)^{Sc}Δ32–88(2P2W) and moPrP(3F4)^{Sc}Δ32–88(2P2G), in N2aC24L1-3 cells (Fig. 7B). These PK-resistant isoforms gave rise to doublet non-glycosylated and mono-glycosylated bands that were very similar to those of moPrP(3F4)^{Sc}Δ32–88 (Fig. 7B), further indicating that the proline residues are not essential for the pre-OR region to form a PK-resistant structure in N2aC24L1-3 cells. IBL-N antibodies failed to detect these mutant proteins on Western blotting since the substitutions disrupted the IBL-N epitope (Fig. 7C).

Positively Charged Lysine Residues, Particularly those Located at Codons 24 and 27, are Important for the Pre-OR Residues 23–31 to Form a PK-resistant Structure in Prion-infected N2a Cells

To gain insights into the role of the lysine residues for the pre-OR residues 23–31 to form a PK-resistant structure, one or two of the lysine residues were changed into alanine residues in moPrP(3F4) Δ32–88(K23A), moPrP(3F4) Δ32–88(K24A), moPrP(3F4) Δ32–88(K27A), moPrP(3F4) Δ32–88(K23,24A), moPrP(3F4) Δ32–88(K23,27A) and moPrP(3F4) Δ32–88(K24,27A) (Fig. 8A). Western blotting with 3F4 antibodies showed that all the mutant proteins were converted into PK-resistant isoforms in N2aC24L1-3 cells, and that all the mutant isoforms gave rise to doublet non-glycosylated and mono-glycosylated bands (Fig. 8B). MoPrP(3F4)^{Sc}Δ32–88(K23A),

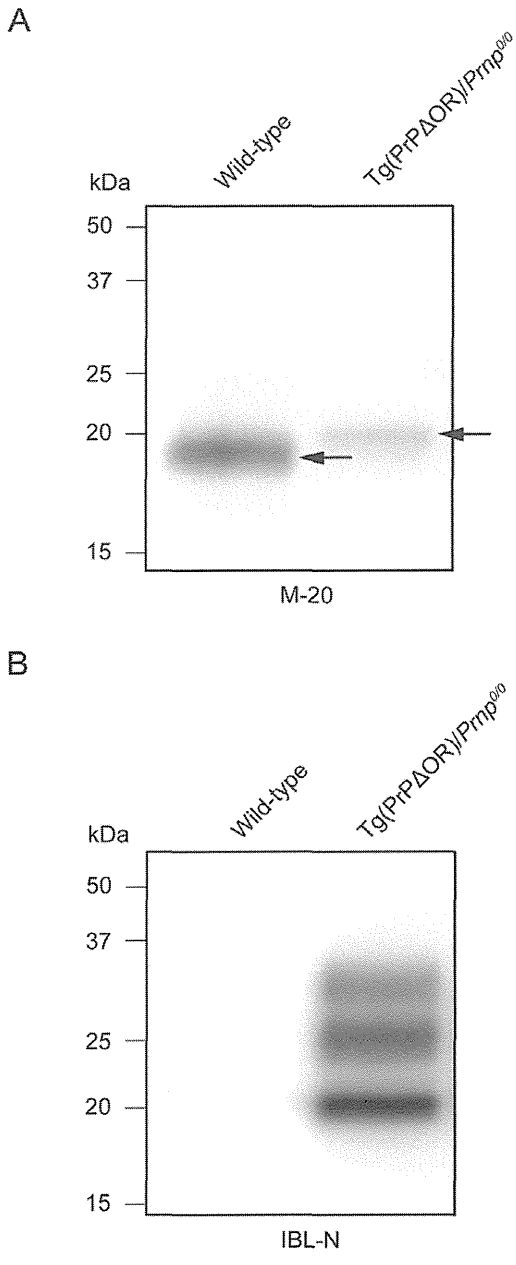

Figure 4. The pre-OR region of PrP^{Sc}ΔOR is PK-resistant. (A) The brain homogenates of terminally ill wild-type and tg(PrPΔOR)/*Prnp*$^{0/0}$ mice were treated with PNGase F after digestion with PK, and subjected to immunoblotting with M-20 anti-PrP antibodies. The deglycosylated PK-resistant band of PrP^{Sc}ΔOR was higher in molecular size than that of full-length PrP^{Sc}. Arrows indicates PK-resistant deglycosylated PrPs. (B) The brain homogenates from terminally ill wild-type and tg(PrPΔOR)/*Prnp*$^{0/0}$ mice were digested with PK, and subjected to immunoblotting with N-terminus-specific IBL-N anti-PrP antibody. The IBL-N antibodies recognized the PK-resistant PrPs from PrP^{Sc}ΔOR but not from full-length PrP^{Sc}.
doi:10.1371/journal.pone.0043540.g004

moPrP(3F4)^{Sc}Δ32–88(K24A) and moPrP(3F4)^{Sc}Δ32–88(K27A) gave rise to the doublet bands with similar molecular size to those of moPrP(3F4)^{Sc}Δ32–88 with the PK-resistant pre-OR residues (Fig. 8B). However, similarly to that of moPrP(3F4)^{Sc}Δ32–88(3K3A) with the PK-sensitive pre-OR residues, the upper band of the doublet from moPrP(3F4)^{Sc}Δ32–88(K24,27A) was reduced in its molecular size and migrated very closely to the lower band (Fig. 8B). MoPrP(3F4)^{Sc}Δ32–88(K23,24A) and moPrP(3F4)^{Sc}Δ32–88(K23,27A) showed the upper band with an intermediate molecular size (Fig. 8B). These results suggest that the number and position of the lysine residues might be important for the pre-OR region of moPrP(3F4) Δ32–88 to become PK-resistant in N2aC24L1-3 cells. In particular, the substitution of two lysine residues located at codons 24 and 27 affected the ability of the pre-OR region in moPrP(3F4) Δ32–88 to form a PK-resistant structure in N2aC24L1-3 cells as strongly as the substitution of all of the three lysine residues did. IBL-N antibodies recognized the upper band of the doublets from all the mutant isoforms except for moPrP(3F4)^{Sc}Δ32–88(K24,27A), probably because the IBL-N epitope was disrupted in moPrP(3F4) Δ32–88(K24,27A), as in moPrP(3F4) Δ32–88(3K3A) (Fig. 8C).

We also replaced all of the lysine residues with positively charged arginine residues in moPrP(3F4) Δ32–88(3K3R) (Fig. 8A). This mutant protein was converted into moPrP(3F4)^{Sc}Δ32–88(3K3R) in N2aC24L1-3 cells and the isoform gave rise to doublet non-glycosylated and mono-glycosylated bands with similar molecular size to those of moPrP(3F4)^{Sc}Δ32–88 with the PK-resistant pre-OR residues (Fig. 8B). The upper band of the doublet was weakly detected by IBL-N antibodies (Fig. 8C). These results indicate that positive charges might play an important role for the pre-OR region of moPrP(3F4) Δ32–88 to become PK-resistant in N2aC24L1-3 cells.

Discussion

Lines of evidence indicate that the N-terminal region of PrP is involved in the susceptibility of mice to prions. Tg(PrPΔ32–93)/*Prnp*$^{0/0}$ and tg(PrPΔ23–88)/*Prnp*$^{0/0}$ mice, which lack the N-terminal residues 32–93 or 23–88, respectively, developed the disease with markedly elongated incubation times after infection with RML prions [9,10]. Moreover, *Prnp*$^{0/0}$ mice expressing PrP with further deletion in the N-terminal domain up to residue 106 from residue 32, or PrPΔ32–106, were free of the disease even after inoculation with RML prions [15]. In contrast, no extended incubation times were observed in tg(PrPΔ32–80)/*Prnp*$^{0/0}$ mice infected with RML prions [16]. PrPΔ32–93 and PrPΔ23–88 lack all or most of the OR region, respectively. However, PrPΔ32–80 still contains one intact octapeptide sequence in the OR region. This suggested that lack of the OR region from PrP could result in the decreased susceptibility to RML prions in the mice. However, in the present study, we observed no extended incubation times in tg(PrPΔOR)/*Prnp*$^{0/0}$ mice, which express PrP lacking only the OR region, after infection with RML prions. The expression level of PrPΔOR in the brain was lower than the reported level of PrPΔ32–93 or PrPΔ23–88 [9,10]. Taken together, these results indicate that, although deletion of the OR region alone from PrP barely affects the susceptibility to RML prions, a large deletion including the OR region in the N-terminal domain could result in remarkable reduction in the susceptibility of mice to RML prions.

We observed different pathogenesis between the brains and spinal cords of terminally ill tg(PrPΔOR)/*Prnp*$^{0/0}$ mice. PrP^{Sc}ΔOR and prion infectivity in the brains were lower than those in control wild-type mice. Astrogliosis in the brains was also milder than that in control wild-type mice. However, in the spinal cords, PrP^{Sc}ΔOR, prion infectivity and astrogliosis were observed similarly to control wild-type mice. These results clearly indicate that, while the OR region is not essential for conversion; its deletion affects conversion taking place in the brain. Moreover, infected tg(PrPΔOR)/*Prnp*$^{0/0}$ mice developed an unusual symp-

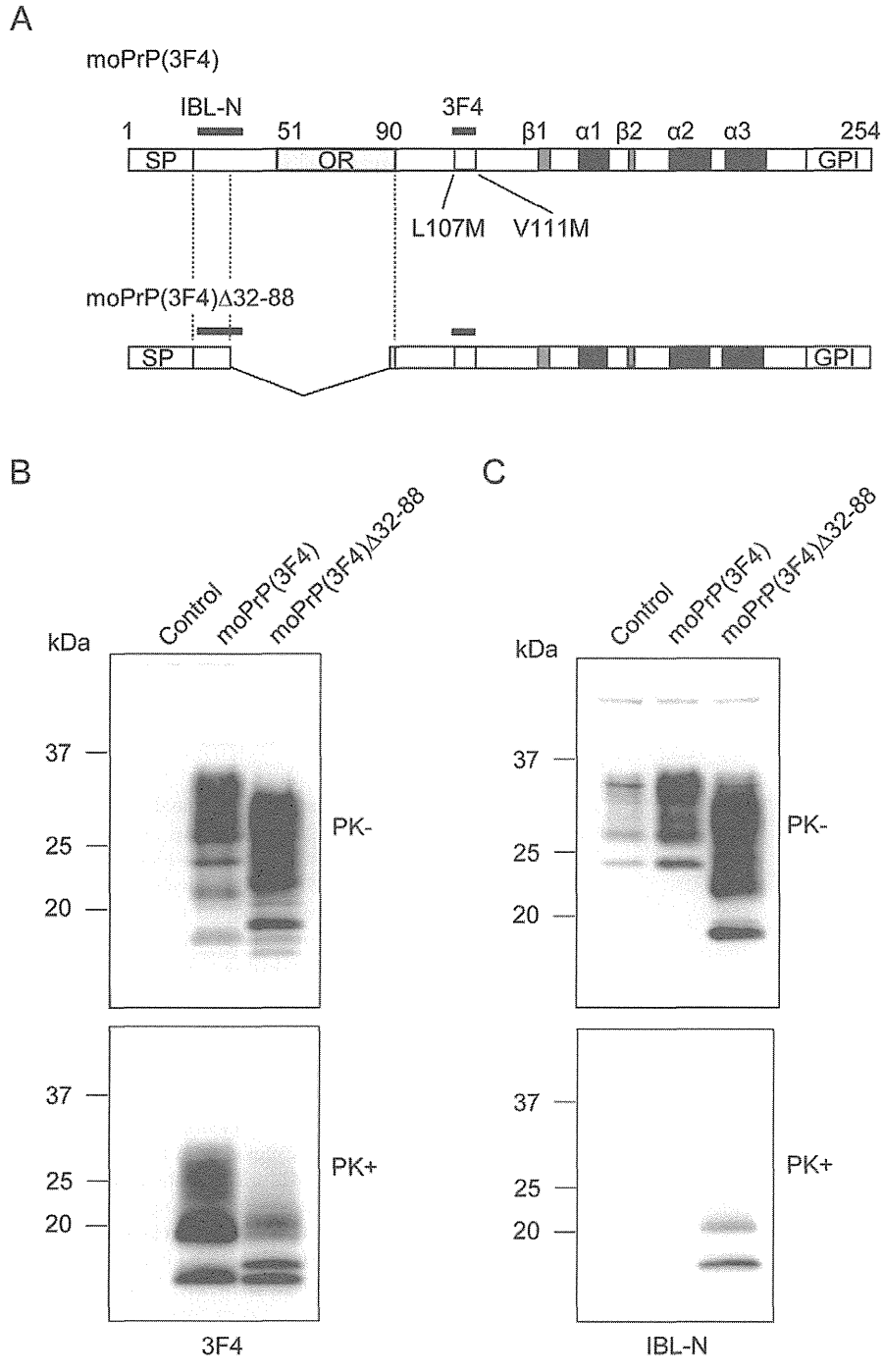

Figure 5. PK-resistant pre-OR residues 23–31 of PrP^{Sc}Δ32–88 generated in prion-infected N2a cells. (A) Schematic diagrams of moPrP(3F4) and moPrP(3F4) Δ32–88. Arabic numbers represent the codon numbers. SP, signal peptide; OR, octapeptide repeat; GPI, GPI anchor signal; α, α-helix; β, β-strand. (B, C) Western blotting of N2aC24L1-3 cells transfected with control pcDNA3.1(+), pcDNA3.1-moPrP(3F4), and pcDNA3.1-moPrP(3F4) Δ32–88 using 3F4 (B) or IBL-N anti-PrP antibodies (C). The cell lysates were treated with PK at 5 μg/ml and then subjected to Western blotting. Both moPrP(3F4) and moPrP(3F4) Δ32–88 were converted to the PK-resistant isoforms, $moPrP^{Sc}$(3F4) and $moPrP^{Sc}$(3F4) Δ32–88, respectively. However, IBL-N anti-PrP antibody reacted only with the PK-resistant fragments of $moPrP^{Sc}$(3F4) Δ32–88.
doi:10.1371/journal.pone.0043540.g005

tom of foreleg paresis, indicating that deletion of the OR region also modifies clinical signs. These unusual phenotypes were also reported in infected tg(PrPΔ32–93)/$Prnp^{0/0}$ mice. This indicates that lack of the OR region from PrP induces such unusual phenotypes in mice after infection with RML prions, as observed in infected tg(PrPΔOR)/$Prnp^{0/0}$ and tg(PrPΔ32–93)/$Prnp^{0/0}$ mice. However, compared to the levels of PrP^{Sc}ΔOR and prion infectivity in the brains of tg(PrPΔOR)/$Prnp^{0/0}$ mice, the reported